

1 **Quantitative phosphoproteomic analysis of acquired cancer drug**
2 **resistance to pazopanib and dasatinib**
3
4
5
6

7 Simon Vyse^{1*}, Frank McCarthy^{1*}, Malgorzata Broncel^{1*#}, Angela Paul², Jocelyn P Wong¹,
8 Amandeep Bhamra² and Paul H Huang^{1,3}.
9

10
11
12
13 **Affiliations:**

14
15 ¹Division of Cancer Biology and ²Proteomics Core Facility, The Institute of Cancer Research,
16 London, SW3 6JB, UK.
17

18
19
20 *These authors contributed equally to this work.

21 #Current address: The Francis Crick Institute, 1 Midland Road, London NW1 1AT, UK.
22

23 ³Correspondence:

24 Paul H Huang
25 Division of Cancer Biology
26 The Institute of Cancer Research
27 London SW3 6JB
28 United Kingdom
29 Email: paul.huang@icr.ac.uk
30 Tel: +44 207 153 5554
31

32 **Running title:** Phosphoproteomics of pazopanib and dasatinib resistance.

33 **Keywords:** Phosphoproteomics, kinase inhibitors, drug resistance, pazopanib, dasatinib,
34 cell signalling
35
36
37
38
39
40
41
42
43
44
45
46
47

48 **Abstract**

49

50 Acquired drug resistance impacts the majority of patients being treated with tyrosine kinase
51 inhibitors (TKIs) and remains a key challenge in modern anti-cancer therapy. The lack of
52 clinically effective therapies to overcome resistance represents an unmet need.
53 Understanding the signalling that drives drug resistance will facilitate the development of
54 new salvage therapies to treat patients with secondary TKI resistance. In this study, we
55 utilise mass spectrometry to characterise the global phosphoproteomic alterations that
56 accompany the acquisition of resistance to two FDA-approved TKIs, pazopanib and
57 dasatinib, in the A204 rhabdoid tumour cell line. Our analysis finds that only 6% and 9.7% of
58 the quantified phosphoproteome is altered upon the acquisition of pazopanib and dasatinib
59 resistance respectively. Pazopanib resistant cells display elevated phosphorylation in
60 cytoskeletal regulatory pathways while dasatinib resistant cells show an upregulation of the
61 insulin receptor/IGF-1R signalling pathway. Drug response profiling rediscovers several
62 previously reported vulnerabilities associated with pazopanib and dasatinib resistance and
63 identifies a new dependency to the second generation HSP90 inhibitor NVP-AUY-922. This
64 study provides a useful resource detailing the candidate signalling determinants of acquired
65 TKI resistance; and reveals a therapeutic approach of inhibiting HSP90 function as a means
66 of salvage therapy to overcome pazopanib and dasatinib resistance.

67

68

69

70

71

72

73

74

75

76

77

78

79

80

81

82

83 **Significance**

84 Pazopanib and dasatinib are tyrosine kinase inhibitors (TKIs) approved for the treatment of
85 multiple cancer types. Patients who are treated with these drugs are prone to the
86 development of drug resistance and consequently tumour relapse. Here we use quantitative
87 phosphoproteomics to characterise the signalling pathways which are enriched in cells that
88 have acquired resistance to these two drugs. Furthermore, targeted drug screens were used
89 to identify salvage therapies capable of overcoming pazopanib and dasatinib resistance.
90 This data advances our understanding of the mechanisms of TKI resistance and highlights
91 candidate targets for cancer therapy.

92

93 **Introduction**

94 Tyrosine kinase inhibitors (TKIs) have emerged as a major class of anti-cancer agents that
95 display efficacy in a range of tumour types including lung cancer, chronic myeloid leukaemia
96 (CML) and gastrointestinal stromal tumours (GIST) [1, 2]. However efficacy is often short-
97 lived with the majority of patients going on to develop acquired resistance and tumour
98 recurrence after prolonged drug treatment [3]. Studies in cell line models have revealed
99 several major mechanisms of resistance that have been clinically observed, including the
100 acquisition of drug resistant mutations in the target kinase, activation of bypass signalling
101 pathways and phenotypic alterations such as epithelial-mesenchymal-transition (EMT) [3-6].
102 These drug resistant cells arise either from selection of pre-existing clones within a
103 heterogeneous tumour cell population or through the adaptation and subsequent evolution of
104 drug-tolerant persister cells [7, 8]. Given that most patients who progress on TKI treatment
105 have limited options for subsequent lines of therapy, there is an urgent need to develop
106 effective salvage therapies to treat patients whose tumours relapse as a result of acquired
107 drug resistance.

108

109 Pazopanib and dasatinib are multi-target TKIs that inhibit a distinct but overlapping spectrum
110 of tyrosine kinases [9-12]. Pazopanib is approved for advanced soft tissue sarcoma and

111 renal-cell carcinoma [13, 14] while dasatinib is licensed for the treatment of CML and
112 Philadelphia chromosome-positive acute lymphoblastic leukaemia (ALL) [15, 16]. Of note,
113 the mechanisms of acquired resistance to pazopanib are poorly characterised in part
114 because there are very few cell line models that harbour intrinsic sensitivity to this drug [17].
115 Despite the largely distinct target selectivity profiles of these two drugs, we have recently
116 demonstrated that in the context of the SMARCB1-deficient rhabdoid tumour cell line A204,
117 acquired resistance to these two compounds is associated with the downregulation of a
118 common target PDGFR α [12]. This acquired resistance could be overcome by the inhibition
119 of bypass signalling initiated by the FGFR1 kinase with inhibitors such as BGJ398, AZD4547
120 and ponatinib as salvage therapy [12].

121

122 Although our laboratory was able to identify common molecular alterations in PDGFR α and
123 FGFR1 in the dasatinib- and pazopanib-resistant A204 cell lines, gene expression and copy
124 number analyses of these cells have revealed clear differences between their molecular
125 profiles [12]. For instance, the dasatinib-resistant cells harboured additional gains on
126 chromosome 17 and losses in chromosome 13 which were not observed in the pazopanib-
127 resistant line [12]. These differences suggest that there are likely to be additional
128 dependencies associated with acquired resistance to dasatinib and pazopanib which can be
129 exploited for cancer therapy. Furthermore, the phosphotyrosine (pTyr)-based proteomics
130 employed in our previous study was only able to identify <5 tyrosine phosphorylated proteins
131 that were upregulated in the two TKI resistant cell lines [12], limiting our ability to determine
132 the signalling pathways enriched as a result of acquired drug resistance. The lack of
133 significantly upregulated pTyr-containing proteins raises the possibility that the major
134 alterations associated with drug resistance in the A204 cells may instead be driven by
135 phosphoserine (pSer) and phosphothreonine (pThr) signalling events.

136

137 In this study we employ a global phosphoproteomics analysis strategy to identify pSer/pThr
138 signalling alterations enriched in the pazopanib- (PazR) and dasatinib-resistant (DasR) A204

139 cell lines. In addition, we perform a targeted drug profiling analysis to determine new
140 vulnerabilities associated with pazopanib and dasatinib resistance in these cells; with the
141 goal of identifying additional salvage therapy candidates to treat patients who have acquired
142 resistance to these drugs. Phosphoproteomics has been extensively used to reveal
143 signalling pathways driving resistance to multiple TKIs including the approved drugs
144 erlotinib, lapatinib, imatinib and sorafenib among others [18-23]. More recently, the value of
145 utilising small panels of targeted drugs directed against key regulators of cancer cell survival
146 to screen for combinations to overcome acquired drug resistance has been successfully
147 demonstrated in lung cancer [24]. Here we utilise these two approaches to determine the
148 signalling pathways which are enriched in pazopanib- and dasatinib-resistant cells and
149 uncover a new vulnerability to the HSP90 inhibitor NVP-AUY-922 which has utility in
150 overcoming acquired resistance to these TKIs.

151

152 **Methods**

153 Cell culture and derivation of acquired resistant sublines

154 Cells were cultured in DMEM media supplemented with 10% FBS, 2mM glutamine,
155 100units/ml penicillin and 100mg/ml streptomycin in 95% air, 5% CO₂ atmosphere at 37°C.
156 For SILAC experiments, A204 cells and resistant sublines were cultured in SILAC DMEM
157 media (Thermo Fisher Scientific) supplemented with light lysine and arginine (R0K0) (Sigma)
158 and heavy lysine and arginine (R10K8) (Goss Scientific), respectively. To generate resistant
159 sublines, A204 cells were grown initially in DMEM media containing Dasatinib and
160 Pazopanib (LC laboratories) at a concentration of 500nM [12]. The drug was incremented
161 when the cells had proliferated to near confluency alongside minimal visible cell death. Drug
162 concentration was incremented from 2µM to 3µM and 5µM in a stepwise manner over 6
163 weeks. A final drug concentration of 5µM was maintained in resistant cells. Media and drug
164 were replenished twice weekly.

165

166

167

168 Cell Viability Assays

169 Cells (2,000/well) were seeded in a 96-well plate and treated with inhibitors at the indicated
170 drugs and doses for 72 hr prior to assessment of cell viability using Cell Titre Glo (Promega),
171 following the manufacturer's recommendations. IC₅₀ data were generated from dose-
172 response curves fitted using a four-parameter regression fit in GraphPad Prism 6 software.
173 Inhibitors used in this study include Gefitinib, Rociletinib, Lapatinib, Neratinib, Sorafenib,
174 Ceritinib, Crizotinib, Pazopanib, Sunitinib, Dasatinib, Ponatinib, AZD4547, Bosutinib,
175 BEZ235, Trametinib, NVP-AUY-922, Imatinib (LC laboratories) AZD9291, PF-562271,
176 Palbociclib, BGJ398, MK2206, AZD5363 (Selleck Chemicals), BX-795, MRT67307 (Sigma-
177 Aldrich), JQ1 (Cayman Chemical Company), DDR1-in-1 (Tocris), CCT244747 (ICR).

178

179 Colony formation assays

180 Cells were seeded at low density (10,000 / well) in 6 well plates and after 24h were treated
181 with inhibitors at the indicated doses for a duration of 2 weeks. Media containing inhibitors
182 was replenished every 72h. Following this, cells were fixed using Carnoy's Fixative (3:1
183 methanol: acetic acid) and stained with 1% crystal violet solution (Sigma-Aldrich).

184

185 Phosphoproteomic enrichment and sample preparation

186 Phosphoproteomic analysis was performed as previously described [25] with the following
187 modifications: SILAC labelled cells (biological triplicates) were lysed in 8M urea and equal
188 amounts of heavy (DasR or PasR cells) and light (parental cells) lysates were mixed prior to
189 reduction, alkylation and trypsin digestion. Peptides were desalted on a C18 cartridge, eluted
190 with 25% acetonitrile and lyophilised to dryness. The sample was reconstituted with 400 µl of
191 IP buffer (100 mM Tris, 100 mM NaCl, 0.3% NP-40, pH 7.4) and the pH was adjusted to 7.4.
192 After immuno-precipitation with pTyr100, pTyr1000 (Cell Signaling Technology) and 4G10
193 (Merck Millipore) for the phosphotyrosine-containing peptides, which were used in a prior
194 study [12], the supernatant was subjected to phosphopeptide enrichment. 2 mg of cell lysate

195 from the supernatant was enriched for phosphopeptides using sequential immobilized metal
196 affinity chromatography (IMAC) on FeCl₃ charged NTA beads as previously described [25].

197

198 A further 2 mg of cell lysate from the supernatant was separately enriched for
199 phosphopeptides using TitanSphere Phos-TiO₂ spin tips (GL Sciences). Spin tips were
200 conditioned using 2 x 20 µl 80% acetonitrile/0.4% trifluoroacetic acid solution, followed by
201 equilibration at with 20 µl 60% acetonitrile/0.3% trifluoroacetic acid/25% lactic acid. Tips
202 were spun at 3000 x g for 2 minutes between each conditioning or equilibration step. The
203 starting peptide sample was vacuum dried and reconstituted in 50 µl 0.1% trifluoroacetic
204 acid solution. The reconstituted sample was mixed with 150 µl 60% acetonitrile/0.3%
205 trifluoroacetic acid/25% lactic acid, added to an equilibrated spin tip and spun at 1000 x g for
206 10 mins. The flow through was collected and applied an additional two more times to the
207 same spin tip to enhance adsorption of phosphopeptides. Following this, the flow through
208 was then applied to a new spin tip and the same enrichment process was followed and
209 analysed separately. After binding of phosphopeptides, spin tips were rinsed twice with 20 µl
210 60% acetonitrile/0.3% trifluoroacetic acid/lactic acid and five times with 20 µl of 80%
211 acetonitrile/0.4% trifluoroacetic acid and spun at 3000 x g for 2 minutes between each step.
212 Phosphopeptides were eluted using 2 x 50 µl of 5% NH₄OH solution and 1 x 50 µl
213 pyrrolidine. Eluates were combined and vacuum dried before LC-MS/MS analysis.

214

215 Liquid Chromatography-Tandem Mass Spectrometry (LC-MS/MS)

216 For IMAC-enriched samples, reversed phase chromatography was performed on eluted
217 peptides using a Dionex UltiMate 3000 RSLC nano system (Thermo Fisher Scientific). The
218 phosphopeptide-enriched eluates were analysed as 6 µL injections, and loaded on to a
219 Acclaim PepMap100 C18 trap cartridge trap cartridge at 8 µL/min 2% acetonitrile/0.1%
220 trifluoroacetic acid (0.5 mm i.d. x 5 mm, 5 µm bead size, 100 Å pore size; loaded in a bi-
221 directional manner). Peptides were then resolved on a 75 µm I.D. 15 cm C18 packed emitter

222 column (3 μm particle size; NIKKYO TECHNOS CO.,LTD). Phosphopeptide-enriched
223 samples were run over 125 min using a three-step gradient of 96:4 to 65:35 buffer A:B (t = 0
224 min 4% B, 5 min 4% B, 14 min 10% B, 118 min 35% B, 125 min 50% B) at 250 nL/min.
225 Peptides were ionised by electrospray ionisation using 1.8 kV applied immediately pre-
226 column via a microtee built into the nanospray source. Sample was infused into an LTQ
227 Velos Orbitrap mass spectrometer (Thermo Fisher Scientific) directly from the end of the
228 tapered tip silica column (6-8 μm exit bore). The ion transfer tube was heated to 275°C and
229 the S-lens set to 60%. MS/MS were acquired using data dependent acquisition based on a
230 full 30,000 resolution FT-MS scan with preview mode disabled and no internal lock mass
231 was used. The top 10 most intense ions were fragmented using enhanced ion trap scans.
232 Precursor ions with unknown or single charge states were excluded from selection.
233 Automatic gain control was set to 1,000,000 for FT-MS and 30,000 for IT-MS/MS, full FT-MS
234 maximum inject time was 500 ms and normalised collision energy was set to 35% with an
235 activation time of 10 ms. Total lysate peptides were subjected to wideband activation to co-
236 fragment precursor ions undergoing neutral loss of up to -20 m/z from the parent ion,
237 including loss of water/ammonia. Multistage activation (MSA) was used to target
238 phosphoserine/threonine peptides by fragmenting precursor ions undergoing neutral loss of
239 32.70, 49.00, 65.40 and 98.00 m/z, corresponding to neutral loss of phosphate, if observed
240 in the top 3 most intense fragment ions. MS/MS was acquired for selected precursor ions
241 with a single repeat count acquired after 8 s delay followed by dynamic exclusion with a 10
242 ppm mass window for 45 s based on a maximal exclusion list of 500 entries.
243 The equivalent of 2 μg of total lysate was also run according to the above conditions to
244 measure the total proteome for subsequent normalisation of phosphoproteomic data. The
245 total lysates were run over 245 min using a three-step gradient of 96:4 to 65:35 buffer A:B (t
246 = 0 min 4% B, 5 min 4% B, 45.0 min 10% B, 230.0 min 35% B, 245.0 min 50% B) and the
247 top 20 most intense ions were fragmented by collision-induced dissociation and analysed
248 using normal ion trap scans as described above.

249 For TiO₂-enriched samples, peptides were resolved on a 75 µm I.D. 50 cm C18 Easy-Spray
250 packed emitter column (2 µm particle size; PepMap RSLC, Thermo Fisher Scientific) over
251 240 min using a multi-step gradient of buffers A:B (t=0 min 5% B, t=5.5 min 4% B, t= 45 min
252 10% B, t = 175 min 25% B, t = 245 min 50% B, t= 250 min, 95% B, t= 255 min, 95% B, t =
253 260 min 4% B, t= 280 4% B) (buffer A: 2% acetonitrile/0.1% formic acid; buffer B: 80%
254 acetonitrile/0.1% formic acid) at 250 nL/min. Peptides were ionised by electrospray
255 ionisation using 2.3 kV applied using the Easy-Spray ion Source. Sample was infused into a
256 Q-Exactive HF mass spectrometer (Thermo Fisher Scientific) directly from the packed
257 emitter (5 µm exit bore). The ion transfer tube was heated to 275°C and the S-lens set to
258 50%. MS/MS were acquired using data dependent acquisition based on a full FT-MS scan
259 from 350 to 1850 m/z at 120,000 resolution, with a target Automatic Gain Control (AGC)
260 value of 3,000,000 and a maximum injection time of 50 ms. No internal lock mass calibrant
261 was used. The top 15 most intense ions were fragmented by higher energy collision-
262 induced dissociation (HCD) and dynamically excluded for 30 s. The normalised collision
263 energy was set to 32 with an activation time of 10 ms. Precursor ions with unknown or
264 single charge states were excluded from selection. Fragmented ions were scanned in the
265 FT-Orbitrap at 60,000 resolution (selected first mass at 100 m/z) with a target AGC value of
266 50,000 and a maximum injection time of 100 ms.

267

268 Data analysis

269 The data were processed with MaxQuant [26] (version 1.5.5.1) and the peptides were
270 identified (maximal mass error = 6 ppm and 20 ppm for precursor and product ions,
271 respectively) from the MS/MS spectra searched against human UniProt database using
272 Andromeda [27] search engine. The following peptide bond cleavages: arginine or lysine
273 followed by any amino acid (a general setting referred to as Trypsin/P) and up to two missed
274 cleavages were allowed. SILAC based experiments in MaxQuant were performed using the
275 built-in quantification algorithm [26] with minimal ratio count = 2 and enabled 'Requantify'
276 feature. For each of the three biological replicate experiments, two technical replicates of the

277 IMAC-phosphopeptide enrichment; two technical replicates of the TiO₂-phosphopeptide
278 enriched samples; and three technical replicates of the total proteome were analysed.
279 Cysteine carbamidomethylation was selected as a fixed modification whereas methionine
280 oxidation; deamidation of asparagine and glutamine; glutamine to pyro-glutamic acid;
281 acetylation of protein N-terminus; with phospho (STY) as variable modifications for
282 phosphoproteome searches. The false discovery rate was set to 0.01 for peptides, proteins
283 and sites. Other parameters were used as default in the software. “Unique and razor
284 peptides” mode was selected to allow identification and quantification of proteins in groups.
285 Data were further analysed using Microsoft Office Excel 2010 and Perseus [28] (version
286 1.5.5.3). Both phosphoproteomic and proteomic data were filtered to remove potential
287 contaminants and IDs originating from reverse decoy sequences. Proteomic data was also
288 filtered to exclude proteins only identified by site. To account for deviations from a 1:1 mix of
289 heavy:light starting material, the median H/L ratio across the entire proteome dataset was
290 used to normalize the phosphoproteomic dataset. The log₂ values of the H/L ratios were then
291 determined. Phosphorylation sites (STY) were filtered to include only high confidence
292 phosphosite IDs (localization probability ≥ 75%). The dataset was then filtered for only valid
293 quantifiable IDs in at least two out of three biological replicates. The mass spectrometry
294 proteomics data have been deposited to the ProteomeXchange Consortium via the PRIDE
295 [29] partner repository with the dataset identifier PXD005536.

296

297 Bioinformatic analysis

298 Biological replicate overlap and phosphorylated amino acid distribution were analysed within
299 Perseus (1.5.5.1) [28]. The phosphoproteome dataset was then annotated with the
300 PhosphositePlus known sites database [30]. The online tool Venny 2.1
301 (<http://bioinfogp.cnb.csic.es/tools/venny/>) was used to generate Venn diagrams and
302 GraphPad Prism 7.02 was used to generate the pie charts.

303

304 One sample t-tests were performed on SILAC \log_2 ratios to determine significantly different
305 regulated phosphosites; where the null hypothesis was that the phosphopeptide abundances
306 were unchanged and the Log2 SILAC ratio was equal to 0. Those phosphosites that were
307 either two-times up-regulated in the A204 parental (t-test difference < -1) or up-regulated in
308 the PazR or DasR (t-test difference > 1) cells and significantly different ($p < 0.05$) were
309 analysed for enrichment. These data are presented as volcano plots generated in GraphPad
310 Prism 7.02 where the statistical significance ($p < 0.05$) was $-\log_{10}$ transformed (y-axis) and
311 plotted against the t-test difference (x-axis).

312

313 Enrichment analysis was performed using DAVID Bioinformatics Resources 6.8 [31] with
314 human genome as a background dataset. KEGG (Kyoto encyclopedia of genes and
315 genomes) [32], Uniprot keyword and sequence feature categories [33], Interpro protein
316 function analysis [34], SMART (Simple Modular Architecture Research Tool) protein domain
317 [35] and COG (Clusters of Orthologous Groups) Analysis Ontology [36] annotation
318 databases were used for analysis. Protein annotation enrichment analysis of the
319 phosphoproteome dataset was performed using the DAVID functional annotation tool and a
320 modified Fisher Exact Test called EASE (Expression Analysis Systematic Explorer) score,
321 comparing up-regulated phosphorylated proteins of PazR and DasR with their corresponding
322 up-regulated phosphorylated proteins in the A204 parental cell line. A statistical cut off of
323 0.005 was applied. Multiple hypothesis testing was controlled using a Benjamini-Hochberg
324 FDR threshold of 0.1. An intersection size of 3 or more was considered to be enriched. A bar
325 chart of the data was then generated within GraphPad Prism 7.02. Additionally, the DAVID
326 enrichment analysis was subjected to network mapping for visualisation using the application
327 EnrichmentMap 2.2.1 within the Cytoscape 3.4.0 software [37]. Lists of phosphoproteins
328 from enrichment clusters were generated and further investigated using the online
329 application STRING 10.5 [38] to construct protein networks and analyse their associations. If
330 necessary, 5 additional STRING interactors were imputed to the networks to propose

331 possible intact, but not measured, systems. The network images were generated from the
332 STRING output of proteins and their interaction score using Cytoscape 3.4.0.

333

334 For drug screen analysis, clustering was performed and heat maps generated within
335 Perseus as described above across each dose of drug (100 or 500 nM) and cell line (A204
336 parental, DasR and PazR) using cell viability values normalised to DMSO control (n=2 or 3).

337

338 **Results**

339 Characterisation of the phosphoproteome in parental and acquired resistant A204 cells

340 Pazopanib resistant (PazR) and dasatinib resistant cells (DasR) were previously derived
341 from the A204 parental cell line by long-term escalating dose treatment with drug [12]
342 (Figure 1A). Briefly, A204 cells were initially grown in media containing 500nM of pazopanib
343 or dasatinib and the drug dose increased when the cells proliferated to near confluency
344 alongside minimal visible cell death. Drug concentration was then increased from 2µM to
345 3µM and then 5µM in a stepwise manner over 6 weeks. A final drug concentration of 5µM
346 was maintained in resistant cells. We subjected the cell lines to stable isotope labelling with
347 amino acids in cell culture (SILAC) with the PazR and DasR cells being 'heavy labelled' and
348 the parental A204 cell line being 'light labelled' (Figure 1A). Cells were lysed, combined in a
349 1:1 ratio and lysates digested with trypsin. We have performed an analysis of the pTyr
350 phosphoproteome of these cells using phosphopeptide immunoprecipitation of the SILAC
351 labelled cell lysates in a previously reported study [12]. In this current study, the supernatant
352 from this pTyr immunoprecipitation was subjected to either immobilised metal affinity
353 chromatography (IMAC) or titanium dioxide (TiO₂) phosphopeptide enrichment prior to
354 single-shot liquid chromatography tandem mass spectrometry (LC-MS/MS) in biological
355 triplicates (Figure 1B). The mass spectrometry data from both phosphopeptide enrichment
356 strategies were combined and analysed together using the MaxQuant algorithm [26]

357

358 Collectively, we identified 7214 unique phosphorylation sites on 2372 proteins in the
359 PazR/A204 comparison and 7548 unique phosphosites on 2494 proteins in the DasR/A204
360 comparison across all three biological replicates (Figure 1C and Table S1 and S2). In both
361 sets of experiments, analysis of the distribution of phosphorylated residues shows the
362 expected classical distribution of pSer:pThr:pTyr ratios (~90:10:1) as previously reported
363 (Figure S1A) [39]. We observed pTyr sites (~1% of all phosphosites) in the analysis despite
364 prior pTyr phosphopeptide enrichment (Figure S1A), indicating that immunoprecipitation did
365 not deplete all the pTyr-containing peptides in the lysate. This may be the result of
366 previously reported restricted pTyr motifs recognised by anti-phosphotyrosine antibodies
367 used in the immunoprecipitation [40]. Consistent with this idea, a comparative analysis of the
368 identified pTyr sites from the previous immunoprecipitation and the current IMAC/TiO₂
369 enrichment shows the overlap of only 1 phosphorylation site between the two datasets
370 (Figure S2). Comparing our phosphoproteomic datasets with the PhosphoSitePlus database
371 showed that 389 and 394 novel phosphosites were identified in the PazR/A204 and
372 DasR/A204 experiments, respectively (Figure S1B, Table S1 and S2) [30]. The total number
373 of phosphosites identified in our dataset is comparable with previous phosphoproteomic
374 studies (ranging from 2000-5000 phosphosites) where single-shot sample injection into the
375 mass spectrometer was carried out with no additional fractionation [41-45].

376

377 Quantitative phosphoproteomic analysis of pazopanib resistance

378 5420 phosphosites on 1950 proteins were quantified in two or more replicates in the
379 PazR/A204 experiments (Figure 2A). To determine the cellular localisation of
380 phosphorylated proteins which are significantly upregulated in PazR or parental A204 cells,
381 we interrogated our dataset using the Uniprot Keyword database and found that with the
382 exception of the nucleus, phosphorylated proteins across multiple subcellular compartments
383 were increased in PazR cells versus the parental A204 line (Figure 2B). 198 phosphorylation
384 sites on 112 proteins (3.7% of the phosphoproteomic dataset) were significantly upregulated
385 more than 2-times ($>\log_2 +1$) in PazR cells compared to parental A204 cells (Figure 2A).

386 These phosphoproteins that were upregulated in PazR cells were subjected to ontology
387 enrichment analysis which revealed the enrichment of a number of ontology terms
388 associated with cytoskeletal organisation (Figure 2C). These included “actin-binding”, “LIM
389 domain containing”, and “Calponin homology (CH) domain containing” proteins (Figure 3A)
390 [46-49]. LIM domain-containing proteins comprise AJUBA, CRIP2, LASP1, LMP7, MICALL1,
391 PDLIM7 and TGFB111 whilst CH-domain proteins include FLNA, LMO7, MICALL1, NAV2,
392 PLEC and SPECC1 (Figure 3B). This gene ontology enrichment analysis suggests that
393 PazR cells upregulate multiple actin cytoskeletal-regulatory pathways which may play a role
394 in maintaining its drug resistant state.

395

396 122 phosphosites on 71 proteins (2.3% of the dataset) were found to be significantly
397 upregulated ($<\log_2 -1$) in the parental A204 cells compared to the PazR cells (Figure 2A) with
398 up to 40% being nuclear proteins (Figure 2B). Ontology analysis of these phosphorylated
399 proteins identified an enrichment of proteins involved in transcription regulation including the
400 ontology terms “transcription regulation”, “transcription”, “transcription activator” and
401 “transcription repressor” (Figure 2C and Figure 3A). These include the transcription factors
402 ETV6, SOX5, SOX6, KLF3, NFIX and DNA binding proteins DNMT1, CDH8, CDH9 and
403 VGLL4 (Figure 3B). Upon interrogation with the STRING database [38], a subset of these
404 proteins showed a well annotated protein-protein interaction network centred around the
405 HDAC1 protein (Figure 3C). The discovery that the phosphorylation of multiple transcription
406 factors is upregulated in SMARCB1-deficient parental A204 rhabdoid tumour cells is
407 consistent with the role of SMARCB1 in organising nucleosome structures surrounding
408 transcriptional start sites in a genome-wide manner [50].

409

410 Quantitative phosphoproteomic analysis of dasatinib resistance

411 5899 phosphosites on 2086 proteins were quantified in two or more biological replicates in
412 the DazR/A204 experiments (Figure 4A). In contrast to the PazR/A204 dataset, both the
413 DasR and parental A204 cell lines show comparable distribution of upregulated

414 phosphorylated proteins across multiple cellular compartments (Figure 4B). The exception is
415 the nuclear compartment where the parental A204 cells have a slight increase in enrichment
416 over the DasR cells. 279 phosphorylation sites on 157 proteins (4.7% of the dataset) were
417 significantly upregulated more than 2-times in DasR cells compared to parental A204 cells
418 (Figure 4A). Subjecting these upregulated phosphosites to gene ontology enrichment
419 analysis (Figure 4C) finds that the DasR cells shows a distinct spectrum of ontology terms
420 compared to the PazR cells with the enrichment of insulin - and IGF-1R signalling pathway
421 components and PDZ domain containing proteins. The insulin signalling pathway cluster
422 includes the proteins ACACA, ARAF, FASN, IRS1, PRKAR1B, PRKAR2B, RPS6KA1,
423 RPS6KB1 and SHC1 which together form a functional protein-protein interaction network
424 (Figure 5). PDZ domain containing proteins that are upregulated in DasR cells include
425 proteins with a range of cellular functions such as cell migration regulation (AHNAK,
426 AHNAK2, SCRIB), cytoskeletal and tight junction proteins (MYO18A and TJP2), and the
427 sodium/hydrogen exchange cofactor SLC9A3R1 (Figure 5A and B).

428

429 294 phosphorylation sites on 157 proteins (5% of the dataset) were found to be upregulated
430 in the parental A204 versus the DasR cells (Figure 4A). Enriched ontology terms include
431 SH3 domain containing proteins (Figure 4C) which play a role in small GTPase regulation
432 and comprise key signalling proteins ARHGEF26, ASAP1, ASAP2, FNBP1L and SRGAP1
433 (Figure 5A and B). Similar to the PazR/A204 dataset, there was an enrichment of
434 transcriptional regulatory terms which include “transcription repressor” and “interferon
435 regulatory factor” (Figure 4C). These include the transcription factors ETV6, NFATC1,
436 ZNF521 and transcriptional repressors NCOR1, TLE4 and SUDS3 (Figure 5). A subset of
437 these proteins feature as part of a protein-protein interaction network centred around the
438 HDAC3 protein (Figure 5C). The observation that protein-protein interaction networks
439 involving the histone deacetylases (HDACs) are enriched in A204 parental cells in both the
440 PazR/A204 and DasR/A204 experiments (Figure 3C and 5C) is consistent with recent

441 preclinical reports that HDAC inhibitors have therapeutic utility in reducing the proliferation of
442 rhabdoid tumour cells including the A204 line [51-53].

443

444 Comparison of PazR and DasR phosphoproteomic datasets

445 A comparison between the two phosphoproteomic datasets revealed a 70.5% overlap with
446 4683 phosphorylation sites quantified across both resistant cell lines (Figure 6A). Taken
447 together, we find that 21.6% of the phosphoproteome is significantly altered upon the
448 acquisition of secondary resistance in PazR and/or DasR sublines versus the parental A204
449 cells (Figure 6B). Supporting our hypothesis that pazopanib and dasatinib induce different
450 cellular reprogramming effects in the A204 cells, only 2.8% and 1.9% of observed
451 phosphosites are similarly up- and down-regulated, respectively, in both datasets (Figure
452 6B). The 34 upregulated and 36 downregulated phosphosites are detailed in Figure 6C-D.

453

454 Drug response profiling identifies new vulnerabilities in drug resistant cells

455 Inspired by a recent targeted screen to identify drugs capable of overcoming bypass
456 signalling pathways associated with acquired TKI resistance in lung cancer [24], we
457 subjected both resistant lines and the parental A204 cells to short term treatment with a
458 focused panel of 28 small molecule inhibitors at two different doses and measured cell
459 viability. This panel comprised of kinase inhibitors targeting the major cellular signalling
460 pathways important for cancer cell survival as well as inhibitors that target the BET
461 bromodomain proteins (JQ1) and the HSP90 protein (NVP-AUY-922) which are currently in
462 advanced clinical trials.

463

464 Two-way hierarchical clustering of the cell viability data demonstrates that the PazR and
465 DasR cells share a more similar drug response profile compared to parental A204 cells
466 (Figure 7A). As shown in our previous study, the two resistant cell lines are highly sensitive
467 to ponatinib treatment [12]. The screen also showed that the dual mTOR/PI3K inhibitor BEZ-
468 235 sensitized both DasR and PazR which recapitulates the findings of a recent report on

469 the use of this drug to overcome pazopanib resistance in patient-derived soft tissue sarcoma
470 cells [54]. We also identify several inhibitors that are only effective in the DasR cells
471 including the MEK inhibitor trametinib and to a lesser extent the CDK4/6 inhibitor palbociclib.
472 MEK inhibitors have been shown to overcome drug resistance induced by the paradoxical
473 activation of the MEK/ERK pathway through the weak binding of dasatinib to BRAF and
474 CRAF [55]. The ability of our targeted screen to rediscover several previously identified
475 vulnerabilities associated with pazopanib and dasatinib resistance provides confidence of
476 the broad applicability of this strategy to identify salvage therapies to sensitize TKI-resistant
477 cells.

478

479 This screen also uncovered a previously undescribed vulnerability of both PazR and DasR
480 cells to the second generation HSP90 inhibitor NVP-AUY-922 which clustered together with
481 ponatinib [56]. Dose response analysis confirms that PazR and DasR cells are sensitive to
482 treatment with NVP-AUY-922 with IC_{50} values of 45.3 ± 14.3 nM and 28.4 ± 5.9 nM,
483 respectively (Figure 7B and C). Long-term colony formation assays show that low dose
484 NVP-AUY-922 (5nM) is capable of not only sensitizing both PazR and DasR cells but also
485 killing parental A204 cells (Figure 7D and E), suggesting that HSP90 inhibitors may be an
486 effective option both as first-line and salvage therapy in rhabdoid tumours.

487

488 **Discussion**

489 This study is, to our knowledge, the first phosphoproteomic analysis of acquired resistance
490 to pazopanib and dasatinib. We show that A204 cells that have acquired secondary
491 resistance to pazopanib (PazR) harbour an enrichment of phosphoproteins that play a role in
492 the regulation of actin cytoskeleton dynamics (Figure 3). These include the LIM domain
493 family of proteins CRIP2, LASP1, MICALL1 and PDLIM7 which have previously been shown
494 to be localised in focal adhesion complexes and play important roles in
495 mechanotransduction signalling [46, 57, 58]. In addition, phosphoproteins that contain the
496 CH domain, a 100 amino acid residue domain that binds to actin filaments, are similarly

497 enriched in PazR cells [48, 49]. Published phosphoproteomic studies have found that
498 melanoma cells with acquired resistance to BRAF inhibitors display elevated levels of
499 phosphoproteins that function in cytoskeletal regulatory pathways [59, 60]. It remains to be
500 determined if the upregulation of cytoskeletal pathways observed in our current study and in
501 the previous melanoma reports is a cause or consequence of the acquisition of drug
502 resistance. However given that this class of proteins is poorly explored as oncology drug
503 targets [61], these phosphoproteomic studies provides a rich source of new candidates for
504 target validation and drug development to overcome drug resistance. In contrast to the PazR
505 cells, acquired resistance to dasatinib in the DasR subline leads to the upregulation of
506 components of the insulin receptor/IGF-1R signalling pathway compared to parental A204
507 cells (Figure 5). Activation of IGF-1R signalling is a well-established bypass mechanism of
508 resistance to many kinase inhibitors including EGFR, HER2, MEK and BRAF inhibitors [62-
509 66]. Furthermore, intrinsic resistance to dasatinib in a panel of non-small-cell lung cancer
510 cell lines has been causally linked to the upregulation of Insulin-like growth factor (IGF)-
511 binding protein-2 (IGFBP2) which act as carrier proteins for the IGF ligands [67]. Our data
512 suggests that the Insulin receptor/IGF-1R pathway is an actionable target for salvage
513 therapy and further investigation to dissect the contribution of components of this pathway to
514 acquired dasatinib resistance is planned.

515

516 One limitation of our study is the relatively modest number of phosphorylation sites identified
517 in our analysis. We quantified ~7000 phosphorylation sites in our experimental dataset
518 (Figure 1B) which is comparable with published reports on single-shot unfractionated
519 samples [42, 44, 45]. In addition, increased precursor ion complexity associated with SILAC
520 labelling results in a decrease in unique phosphopeptide identification [68]. Greater depth of
521 coverage in the phosphoproteome can be achieved with additional pre-fractionation steps
522 [42, 44, 45], and combining orthogonal phosphopeptide enrichment strategies [69, 70].
523 Another limitation of the study is the focus on phosphoproteomic analysis without accounting
524 for protein abundance changes. In the absence of a deep proteome analysis of the resistant

525 and sensitive cell lines, we are unable to distinguish if the phosphorylation changes
526 observed in our dataset are due to alterations in protein phosphorylation stoichiometry or at
527 the level of total protein expression. Notwithstanding these limitations, our study
528 demonstrates that candidate resistance signalling pathways can be readily identified with
529 this approach.

530

531 Our phosphoproteomic analysis finds that acquired resistance to pazopanib and dasatinib
532 leads to a 6.0% and 9.7% change, respectively, in the quantified phosphoproteome
533 compared to parental A204 cells (Figure 2A and 4A). A recent study by Nagata et al.,
534 showed that acquired resistance to the TKI imatinib in a GIST cell line displayed alterations
535 in ~75% of the phosphoproteome when compared to the parental sensitive cell line [21]. In
536 contrast, a phosphoproteomic analysis by Lee et al., of acquired resistance to the TKI
537 lapatinib in a gastric cancer cell line showed that 5% of the phosphoproteome was
538 significantly altered versus the parental cells from which resistance was derived [20]. The
539 low percentage of phosphorylation changes observed in our study may be due to a number
540 of factors. One reason could be that the depth of phosphoproteome coverage is less
541 comprehensive in our analysis and that we are only sampling the most abundant
542 phosphoproteins in the cell, although this is unlikely given that the study by Nagata et al.,
543 identified ~1000 phosphoserine/threonine sites with a 75% difference observed while Lee et
544 al., quantified 6500 phosphosites with only 5% alterations seen. Another contributing factor
545 is that the underlying genomic drivers of the cell lines used in the different studies are
546 distinct. Unlike the GIST and gastric cell lines used in the previous studies, the A204
547 rhabdoid tumour cell line has a very simple genome where the loss of the SWI/SNF
548 chromatin remodelling subunit SMARCB1 is the only known cancer-associated driver [12,
549 71-74]. It is plausible that loss of SMARCB1 may be sufficient to drive acquired TKI
550 resistance with limited alterations in the phosphoproteome. Finally it is also possible that
551 different TKIs reprogram cellular signalling networks to achieve drug resistance using distinct
552 mechanisms [4, 75, 76].

553

554 The targeted drug profiling analysis identified the HSP90 inhibitor NVP-AUY-922 as a novel
555 means to overcome pazopanib and dasatinib resistance (Figure 7). The small molecule
556 inhibitor panel that we employed was designed to block a range of distinct bypass pathways
557 that have previously been associated with TKI resistance [24]. We show that AUY-922 is
558 capable of not only overcoming acquired resistance in the form of salvage therapy, but also
559 has utility when applied in the first-line setting (Figure 7C). HSP90 inhibitors have been
560 deployed as salvage therapy in clinical trials for TKI-resistant lung cancer and GIST with
561 varying results [77, 78]. The rationale for this approach is based on pre-clinical evidence that
562 cancer cells are dependent on HSP90 for stabilising client proteins such as TKI resistance-
563 associated mutants and kinases responsible for driving bypass signalling in cancer cells [79,
564 80]. Consequently inhibition of HSP90 has the potential to simultaneously block multiple
565 resistance mechanisms in the context of salvage therapy [80]. The mechanism for the
566 activity of AUY922 in sensitizing the PazR and DasR cells and the specific client proteins
567 involved in mediating drug sensitivity remain unclear and will be the focus of future studies.

568

569 In summary, we have performed a phosphoproteomic analysis to determine the signalling
570 pathways associated with acquired resistance to pazopanib and dasatinib. We also
571 demonstrate that PazR and DasR cells are sensitive to the HSP90 inhibitor NVP-AUY-922.
572 This study provides a useful resource for future studies investigating the determinants of
573 pazopanib and dasatinib resistance; and identifies a new therapeutic strategy of inhibiting
574 HSP90 function for further evaluation as a means of overcoming pazopanib and dasatinib
575 resistance and tumour recurrence in multiple cancer types.

576

577 **Acknowledgements**

578 This work was supported by grants to PHH from the Institute of Cancer Research, Cancer
579 Research UK (C36478/A19281), Sarcoma UK (003.2014), Royal Marsden Cancer Charity.
580 SV is supported by an ICR studentship.

581

582 **References**

583

584 [1] Lemmon MA, Schlessinger J. Cell signaling by receptor tyrosine kinases. *Cell*.
585 2010;141:1117-34.

586 [2] Levitzki A. Tyrosine kinase inhibitors: views of selectivity, sensitivity, and clinical
587 performance. *Annu Rev Pharmacol Toxicol*. 2013;53:161-85.

588 [3] Sierra JR, Cepero V, Giordano S. Molecular mechanisms of acquired resistance to
589 tyrosine kinase targeted therapy. *Mol Cancer*. 2010;9:75.

590 [4] Gainor JF, Shaw AT. Emerging paradigms in the development of resistance to tyrosine
591 kinase inhibitors in lung cancer. *J Clin Oncol*. 2013;31:3987-96.

592 [5] Xu AM, Huang PH. Receptor tyrosine kinase coactivation networks in cancer. *Cancer*
593 *Res*. 2010;70:3857-60.

594 [6] Vyse S, Howitt A, Huang PH. Exploiting Synthetic Lethality and Network Biology to
595 Overcome EGFR Inhibitor Resistance in Lung Cancer. *J Mol Biol*. 2017.

596 [7] Hata AN, Niederst MJ, Archibald HL, Gomez-Caraballo M, Siddiqui FM, Mulvey HE, et al.
597 Tumor cells can follow distinct evolutionary paths to become resistant to epidermal growth
598 factor receptor inhibition. *Nat Med*. 2016;22:262-9.

599 [8] Ramirez M, Rajaram S, Steininger RJ, Osipchuk D, Roth MA, Morinishi LS, et al. Diverse
600 drug-resistance mechanisms can emerge from drug-tolerant cancer persister cells. *Nat*
601 *Commun*. 2016;7:10690.

602 [9] Kitagawa D, Yokota K, Gouda M, Narumi Y, Ohmoto H, Nishiwaki E, et al. Activity-based
603 kinase profiling of approved tyrosine kinase inhibitors. *Genes Cells*. 2013;18:110-22.

604 [10] Anastassiadis T, Deacon SW, Devarajan K, Ma H, Peterson JR. Comprehensive assay
605 of kinase catalytic activity reveals features of kinase inhibitor selectivity. *Nat Biotechnol*.
606 2011;29:1039-45.

607 [11] Davis MI, Hunt JP, Herrgard S, Ciceri P, Wodicka LM, Pallares G, et al. Comprehensive
608 analysis of kinase inhibitor selectivity. *Nat Biotechnol*. 2011;29:1046-51.

609 [12] Wong JP, Todd JR, Finetti MA, McCarthy F, Broncel M, Vyse S, et al. Dual Targeting of
610 PDGFRalpha and FGFR1 Displays Synergistic Efficacy in Malignant Rhabdoid Tumors. *Cell*
611 *Rep*. 2016;17:1265-75.

612 [13] Motzer RJ, Hutson TE, Cella D, Reeves J, Hawkins R, Guo J, et al. Pazopanib versus
613 sunitinib in metastatic renal-cell carcinoma. *N Engl J Med*. 2013;369:722-31.

614 [14] van der Graaf WT, Blay JY, Chawla SP, Kim DW, Bui-Nguyen B, Casali PG, et al.
615 Pazopanib for metastatic soft-tissue sarcoma (PALETTE): a randomised, double-blind,
616 placebo-controlled phase 3 trial. *Lancet*. 2012;379:1879-86.

617 [15] Talpaz M, Shah NP, Kantarjian H, Donato N, Nicoll J, Paquette R, et al. Dasatinib in
618 imatinib-resistant Philadelphia chromosome-positive leukemias. *N Engl J Med*.
619 2006;354:2531-41.

- 620 [16] Kantarjian H, Shah NP, Hochhaus A, Cortes J, Shah S, Ayala M, et al. Dasatinib versus
621 imatinib in newly diagnosed chronic-phase chronic myeloid leukemia. *N Engl J Med.*
622 2010;362:2260-70.
- 623 [17] Yang W, Soares J, Greninger P, Edelman EJ, Lightfoot H, Forbes S, et al. Genomics of
624 Drug Sensitivity in Cancer (GDSC): a resource for therapeutic biomarker discovery in cancer
625 cells. *Nucleic Acids Res.* 2013;41:D955-61.
- 626 [18] Dazert E, Colombi M, Boldanova T, Moes S, Adametz D, Quagliata L, et al. Quantitative
627 proteomics and phosphoproteomics on serial tumor biopsies from a sorafenib-treated HCC
628 patient. *Proc Natl Acad Sci U S A.* 2016;113:1381-6.
- 629 [19] Yoshida T, Zhang G, Smith MA, Lopez AS, Bai Y, Li J, et al. Tyrosine
630 phosphoproteomics identifies both codrivers and cotargeting strategies for T790M-related
631 EGFR-TKI resistance in non-small cell lung cancer. *Clin Cancer Res.* 2014;20:4059-74.
- 632 [20] Lee YY, Kim HP, Kang MJ, Cho BK, Han SW, Kim TY, et al. Phosphoproteomic analysis
633 identifies activated MET-axis PI3K/AKT and MAPK/ERK in lapatinib-resistant cancer cell
634 line. *Exp Mol Med.* 2013;45:e64.
- 635 [21] Nagata K, Kawakami T, Kurata Y, Kimura Y, Suzuki Y, Nagata T, et al. Augmentation of
636 multiple protein kinase activities associated with secondary imatinib resistance in
637 gastrointestinal stromal tumors as revealed by quantitative phosphoproteome analysis. *J*
638 *Proteomics.* 2015;115:132-42.
- 639 [22] Winter GE, Rix U, Carlson SM, Gleixner KV, Grebien F, Gridling M, et al. Systems-
640 pharmacology dissection of a drug synergy in imatinib-resistant CML. *Nat Chem Biol.*
641 2012;8:905-12.
- 642 [23] Noujaim J, Payne LS, Judson I, Jones RL, Huang PH. Phosphoproteomics in
643 translational research: a sarcoma perspective. *Ann Oncol.* 2016;27:787-94.
- 644 [24] Crystal AS, Shaw AT, Sequist LV, Friboulet L, Niederst MJ, Lockerman EL, et al.
645 Patient-derived models of acquired resistance can identify effective drug combinations for
646 cancer. *Science.* 2014;346:1480-6.
- 647 [25] Iwai LK, Payne LS, Luczynski MT, Chang F, Xu H, Clinton RW, et al.
648 Phosphoproteomics of collagen receptor networks reveals SHP-2 phosphorylation
649 downstream of wild-type DDR2 and its lung cancer mutants. *Biochem J.* 2013;454:501-13.
- 650 [26] Cox J, Mann M. MaxQuant enables high peptide identification rates, individualized
651 p.p.b.-range mass accuracies and proteome-wide protein quantification. *Nat Biotechnol.*
652 2008;26:1367-72.
- 653 [27] Cox J, Neuhauser N, Michalski A, Scheltema RA, Olsen JV, Mann M. Andromeda: a
654 peptide search engine integrated into the MaxQuant environment. *J Proteome Res.*
655 2011;10:1794-805.
- 656 [28] Tyanova S, Temu T, Sinitcyn P, Carlson A, Hein MY, Geiger T, et al. The Perseus
657 computational platform for comprehensive analysis of (prote)omics data. *Nat Methods.*
658 2016;13:731-40.
- 659 [29] Vizcaino JA, Csordas A, Del-Toro N, Dianas JA, Griss J, Lavidas I, et al. 2016 update of
660 the PRIDE database and its related tools. *Nucleic Acids Res.* 2016.

661 [30] Hornbeck PV, Zhang B, Murray B, Kornhauser JM, Latham V, Skrzypek E.
662 PhosphoSitePlus, 2014: mutations, PTMs and recalibrations. *Nucleic Acids Res.*
663 2015;43:D512-20.

664 [31] Huang da W, Sherman BT, Lempicki RA. Systematic and integrative analysis of large
665 gene lists using DAVID bioinformatics resources. *Nat Protoc.* 2009;4:44-57.

666 [32] Kanehisa M, Furumichi M, Tanabe M, Sato Y, Morishima K. KEGG: new perspectives
667 on genomes, pathways, diseases and drugs. *Nucleic Acids Res.* 2017;45:D353-D61.

668 [33] UniProt: the universal protein knowledgebase. *Nucleic Acids Res.* 2017;45:D158-D69.

669 [34] Finn RD, Attwood TK, Babbitt PC, Bateman A, Bork P, Bridge AJ, et al. InterPro in
670 2017-beyond protein family and domain annotations. *Nucleic Acids Res.* 2017;45:D190-D9.

671 [35] Letunic I, Doerks T, Bork P. SMART: recent updates, new developments and status in
672 2015. *Nucleic Acids Res.* 2015;43:D257-60.

673 [36] Tatusov RL, Fedorova ND, Jackson JD, Jacobs AR, Kiryutin B, Koonin EV, et al. The
674 COG database: an updated version includes eukaryotes. *BMC Bioinformatics.* 2003;4:41.

675 [37] Shannon P, Markiel A, Ozier O, Baliga NS, Wang JT, Ramage D, et al. Cytoscape: a
676 software environment for integrated models of biomolecular interaction networks. *Genome*
677 *Res.* 2003;13:2498-504.

678 [38] Szklarczyk D, Morris JH, Cook H, Kuhn M, Wyder S, Simonovic M, et al. The STRING
679 database in 2017: quality-controlled protein-protein association networks, made broadly
680 accessible. *Nucleic Acids Res.* 2017;45:D362-D8.

681 [39] Ubersax JA, Ferrell JE, Jr. Mechanisms of specificity in protein phosphorylation. *Nat*
682 *Rev Mol Cell Biol.* 2007;8:530-41.

683 [40] Tinti M, Nardoza AP, Ferrari E, Sacco F, Corallino S, Castagnoli L, et al. The 4G10,
684 pY20 and p-TYR-100 antibody specificity: profiling by peptide microarrays. *N Biotechnol.*
685 2012;29:571-7.

686 [41] Zahari MS, Wu X, Pinto SM, Nirujogi RS, Kim MS, Fetis B, et al. Phosphoproteomic
687 profiling of tumor tissues identifies HSP27 Ser82 phosphorylation as a robust marker of early
688 ischemia. *Sci Rep.* 2015;5:13660.

689 [42] Lawrence RT, Searle BC, Llovet A, Villen J. Plug-and-play analysis of the human
690 phosphoproteome by targeted high-resolution mass spectrometry. *Nat Methods.*
691 2016;13:431-4.

692 [43] Bensimon A, Schmidt A, Ziv Y, Elkon R, Wang SY, Chen DJ, et al. ATM-dependent and
693 -independent dynamics of the nuclear phosphoproteome after DNA damage. *Sci Signal.*
694 2010;3:rs3.

695 [44] Matheron L, van den Toorn H, Heck AJ, Mohammed S. Characterization of biases in
696 phosphopeptide enrichment by Ti(4+)-immobilized metal affinity chromatography and TiO₂
697 using a massive synthetic library and human cell digests. *Anal Chem.* 2014;86:8312-20.

698 [45] Ruprecht B, Koch H, Medard G, Mundt M, Kuster B, Lemeer S. Comprehensive and
699 reproducible phosphopeptide enrichment using iron immobilized metal ion affinity
700 chromatography (Fe-IMAC) columns. *Mol Cell Proteomics.* 2015;14:205-15.

- 701 [46] Smith MA, Hoffman LM, Beckerle MC. LIM proteins in actin cytoskeleton
702 mechanoresponse. *Trends Cell Biol.* 2014;24:575-83.
- 703 [47] Jarvinen PM, Laiho M. LIM-domain proteins in transforming growth factor beta-induced
704 epithelial-to-mesenchymal transition and myofibroblast differentiation. *Cell Signal.*
705 2012;24:819-25.
- 706 [48] Sjoblom B, Ylanne J, Djinovic-Carugo K. Novel structural insights into F-actin-binding
707 and novel functions of calponin homology domains. *Curr Opin Struct Biol.* 2008;18:702-8.
- 708 [49] Korenbaum E, Rivero F. Calponin homology domains at a glance. *J Cell Sci.*
709 2002;115:3543-5.
- 710 [50] Tolstorukov MY, Sansam CG, Lu P, Koellhoffer EC, Helming KC, Alver BH, et al.
711 Swi/Snf chromatin remodeling/tumor suppressor complex establishes nucleosome
712 occupancy at target promoters. *Proc Natl Acad Sci U S A.* 2013;110:10165-70.
- 713 [51] Muscat A, Popovski D, Jayasekara WS, Rossello FJ, Ferguson M, Marini KD, et al.
714 Low-Dose Histone Deacetylase Inhibitor Treatment Leads to Tumor Growth Arrest and Multi-
715 Lineage Differentiation of Malignant Rhabdoid Tumors. *Clin Cancer Res.* 2016;22:3560-70.
- 716 [52] Kerl K, Ries D, Unland R, Borchert C, Moreno N, Hasselblatt M, et al. The histone
717 deacetylase inhibitor SAHA acts in synergism with fenretinide and doxorubicin to control
718 growth of rhabdoid tumor cells. *BMC Cancer.* 2013;13:286.
- 719 [53] Knipstein JA, Birks DK, Donson AM, Alimova I, Foreman NK, Vibhakar R. Histone
720 deacetylase inhibition decreases proliferation and potentiates the effect of ionizing radiation
721 in atypical teratoid/rhabdoid tumor cells. *Neuro Oncol.* 2012;14:175-83.
- 722 [54] Kim HK, Kim SY, Lee SJ, Kang M, Kim ST, Jang J, et al. BEZ235 (PIK3/mTOR inhibitor)
723 Overcomes Pazopanib Resistance in Patient-Derived Refractory Soft Tissue Sarcoma Cells.
724 *Transl Oncol.* 2016;9:197-202.
- 725 [55] Packer LM, Rana S, Hayward R, O'Hare T, Eide CA, Rebocho A, et al. Nilotinib and
726 MEK inhibitors induce synthetic lethality through paradoxical activation of RAF in drug-
727 resistant chronic myeloid leukemia. *Cancer Cell.* 2011;20:715-27.
- 728 [56] Eccles SA, Massey A, Raynaud FI, Sharp SY, Box G, Valenti M, et al. NVP-AUY922: a
729 novel heat shock protein 90 inhibitor active against xenograft tumor growth, angiogenesis,
730 and metastasis. *Cancer Res.* 2008;68:2850-60.
- 731 [57] Schiller HB, Friedel CC, Boulegue C, Fassler R. Quantitative proteomics of the integrin
732 adhesome show a myosin II-dependent recruitment of LIM domain proteins. *EMBO Rep.*
733 2011;12:259-66.
- 734 [58] Kuo JC, Han X, Hsiao CT, Yates JR, 3rd, Waterman CM. Analysis of the myosin-II-
735 responsive focal adhesion proteome reveals a role for beta-Pix in negative regulation of focal
736 adhesion maturation. *Nat Cell Biol.* 2011;13:383-93.
- 737 [59] Parker R, Vella LJ, Xavier D, Amirkhani A, Parker J, Cebon J, et al. Phosphoproteomic
738 Analysis of Cell-Based Resistance to BRAF Inhibitor Therapy in Melanoma. *Front Oncol.*
739 2015;5:95.

740 [60] Girotti MR, Pedersen M, Sanchez-Laorden B, Viros A, Turajlic S, Niculescu-Duvaz D, et
741 al. Inhibiting EGF receptor or SRC family kinase signaling overcomes BRAF inhibitor
742 resistance in melanoma. *Cancer Discov.* 2013;3:158-67.

743 [61] Patel MN, Halling-Brown MD, Tym JE, Workman P, Al-Lazikani B. Objective
744 assessment of cancer genes for drug discovery. *Nat Rev Drug Discov.* 2013;12:35-50.

745 [62] Cortot AB, Repellin CE, Shimamura T, Capelletti M, Zejnullahu K, Ercan D, et al.
746 Resistance to irreversible EGF receptor tyrosine kinase inhibitors through a multistep
747 mechanism involving the IGF1R pathway. *Cancer Res.* 2013;73:834-43.

748 [63] Guix M, Faber AC, Wang SE, Olivares MG, Song Y, Qu S, et al. Acquired resistance to
749 EGFR tyrosine kinase inhibitors in cancer cells is mediated by loss of IGF-binding proteins. *J*
750 *Clin Invest.* 2008;118:2609-19.

751 [64] Nahta R, Yuan LX, Zhang B, Kobayashi R, Esteva FJ. Insulin-like growth factor-I
752 receptor/human epidermal growth factor receptor 2 heterodimerization contributes to
753 trastuzumab resistance of breast cancer cells. *Cancer Res.* 2005;65:11118-28.

754 [65] Villanueva J, Vultur A, Lee JT, Somasundaram R, Fukunaga-Kalabis M, Cipolla AK, et
755 al. Acquired resistance to BRAF inhibitors mediated by a RAF kinase switch in melanoma
756 can be overcome by cotargeting MEK and IGF-1R/PI3K. *Cancer Cell.* 2010;18:683-95.

757 [66] Denduluri SK, Idowu O, Wang Z, Liao Z, Yan Z, Mohammed MK, et al. Insulin-like
758 growth factor (IGF) signaling in tumorigenesis and the development of cancer drug
759 resistance. *Genes Dis.* 2015;2:13-25.

760 [67] Lu H, Wang L, Gao W, Meng J, Dai B, Wu S, et al. IGFBP2/FAK pathway is causally
761 associated with dasatinib resistance in non-small cell lung cancer cells. *Mol Cancer Ther.*
762 2013;12:2864-73.

763 [68] Ong SE. The expanding field of SILAC. *Anal Bioanal Chem.* 2012;404:967-76.

764 [69] Engholm-Keller K, Hansen TA, Palmisano G, Larsen MR. Multidimensional strategy for
765 sensitive phosphoproteomics incorporating protein prefractionation combined with SIMAC,
766 HILIC, and TiO(2) chromatography applied to proximal EGF signaling. *J Proteome Res.*
767 2011;10:5383-97.

768 [70] Vyse S, Desmond H, Huang PH. Advances in mass spectrometry based strategies to
769 study receptor tyrosine kinases. *IUCrJ.* 2017;4:119-30.

770 [71] Chou TC, Talalay P. Quantitative analysis of dose-effect relationships: the combined
771 effects of multiple drugs or enzyme inhibitors. *Adv Enzyme Regul.* 1984;22:27-55.

772 [72] Johann PD, Erkek S, Zapatka M, Kerl K, Buchhalter I, Hovestadt V, et al. Atypical
773 Teratoid/Rhabdoid Tumors Are Comprised of Three Epigenetic Subgroups with Distinct
774 Enhancer Landscapes. *Cancer Cell.* 2016;29:379-93.

775 [73] Lee RS, Stewart C, Carter SL, Ambrogio L, Cibulskis K, Sougnez C, et al. A remarkably
776 simple genome underlies highly malignant pediatric rhabdoid cancers. *J Clin Invest.*
777 2012;122:2983-8.

778 [74] Huang PH. Targeting SWI/SNF mutant cancers with tyrosine kinase inhibitor therapy.
779 *Expert Rev Anticancer Ther.* 2017;17:1-3.

- 780 [75] Tan AC, Vyse S, Huang PH. Exploiting receptor tyrosine kinase co-activation for cancer
781 therapy. *Drug Discov Today*. 2017;22:72-84.
- 782 [76] Bonanno L, Jirillo A, Favaretto A. Mechanisms of acquired resistance to epidermal
783 growth factor receptor tyrosine kinase inhibitors and new therapeutic perspectives in non
784 small cell lung cancer. *Curr Drug Targets*. 2011;12:922-33.
- 785 [77] Sequist LV, Gettinger S, Senzer NN, Martins RG, Janne PA, Lilenbaum R, et al. Activity
786 of IPI-504, a novel heat-shock protein 90 inhibitor, in patients with molecularly defined non-
787 small-cell lung cancer. *J Clin Oncol*. 2010;28:4953-60.
- 788 [78] Demitri GD, Heinrich MC, Chmielowski B, Morgan JA, George S, Bradley R, et al. An
789 open-label phase II study of the Hsp90 inhibitor ganetespib (STA-9090) in patients (pts) with
790 metastatic and/or unresectable GIST. *J Clin Oncol*. 2011;29:10011.
- 791 [79] Workman P, Burrows F, Neckers L, Rosen N. Drugging the cancer chaperone HSP90:
792 combinatorial therapeutic exploitation of oncogene addiction and tumor stress. *Ann N Y*
793 *Acad Sci*. 2007;1113:202-16.
- 794 [80] Proia DA, Bates RC. Ganetespib and HSP90: translating preclinical hypotheses into
795 clinical promise. *Cancer Res*. 2014;74:1294-300.

796

797 **Figure Legends**

798 **Figure 1. Experimental outline and phosphoproteome dataset overview.** (A) Dose
799 response curve of A204 parental and PazR cells to pazopanib and A204 parental and DasR
800 cells to dasatinib respectively. (B) Schematic of sample preparation workflow. Pazopanib
801 and dasatinib resistant A204 cell lines (PazR & DasR respectively) were generated and
802 heavy SILAC labelled as previously described [12]. A204 parental cells were light SILAC
803 labelled. After cell lysis, either heavy PazR or DasR were mixed 1:1 with light A204 parental
804 lysate then reduced, alkylated and trypsin digested. The resulting peptides underwent
805 phospho-tyrosine (pTyr) peptide immunoprecipitation, data previously published [12]. The
806 supernatant from the immunoprecipitation was further enriched with immobilised metal
807 affinity chromatography (IMAC) or titanium dioxide (TiO₂) prior to liquid chromatography
808 tandem mass spectrometry analysis (LC MS/MS). (C) Venn diagrams show distribution of
809 phosphorylation sites across three biological replicates (R1, R2 and R3) in PazR/A204 and
810 DasR/A204 experiments..

811

812 **Figure 2. Phosphoproteomic profile of PazR versus A204 parental cells.** (A) Volcano
813 plot depicting the phosphoproteome of PazR versus A204 parental cells. All ratios were
814 median-normalised and \log_2 transformed. A one sample t-test was performed where the null
815 hypothesis was equal to 0. The statistical significance was $-\log_{10}$ transformed (y-axis) and
816 plotted against the t-test difference (x-axis). Phosphosites that display at least 2-times
817 increase in PazR (red) or increase in A204 parental (blue) with $p < 0.05$ are indicated.
818 Legend shows percentage of phosphosites that were up-regulated in PazR cells or A204
819 parental cells as well as phosphosites that displayed no change between the two cell lines.
820 (B) Uniprot keyword annotation terms linked to either statistically significant PazR or A204
821 parental up-regulated phosphoproteins generated using the DAVID functional annotation
822 tool [31]. (C) Annotation enrichment analysis of phosphoproteins up-regulated in either the
823 PazR or A204 parental cells compared against the human genome using DAVID. The
824 resultant p values of each term were $-\log_{10}$ transformed. Multiple hypothesis testing was
825 controlled using a Benjamini-Hochburg FDR threshold of 0.1.

826

827 **Figure 3. Biological function analysis of PazR versus A204 parental cells.** (A)
828 Annotation enrichment analysis of PazR and A204 parental up-regulated phosphoproteins
829 using the DAVID functional annotation tool. Network maps represent clusters of annotation
830 terms from different databases with associated function. Nodes represent each term and the
831 connecting line their association; line thickness is number of overlapping proteins. The inner
832 and outer nodes are PazR and A204 parental datasets respectively. Node size represents
833 the number of proteins annotated with that term. The colour intensity of the node represents
834 the significance of enrichment and grey depicts no proteins. (B) Heat map of proteins in
835 network cluster based on the $\log_2(\text{PazR}/\text{A204})$ SILAC ratio. (C) An association network of
836 proteins from the 'transcription' cluster analysed through the STRING application. Blue
837 coloured proteins are from the cluster list and grey are added STRING interactors. Line
838 thickness portrays the STRING calculated association confidence.

839

840 **Figure 4. Phosphoproteomic profile of DasR versus A204 parental cells.** (A) Volcano
841 plot depicting the phosphoproteome of DasR versus A204 parental cells. All ratios were
842 median-normalised and \log_2 transformed. A one sample t-test was performed where the null
843 hypothesis was equal to 0. The statistical significance was $-\log_{10}$ transformed (y-axis) and
844 plotted against the t-test difference (x-axis). Phosphosites that display at least 2-times
845 increase in DasR (red) or increase in A204 parental (blue) with $p < 0.05$ are indicated.
846 Legend shows percentage of phosphosites that were up-regulated in DasR cells or A204
847 parental cells as well as phosphosites that displayed no change between the two cell lines.
848 (B) Uniprot keyword annotation terms linked to either statistically significant DasR or A204
849 parental up-regulated phosphoproteins generated using the DAVID functional annotation
850 tool [31]. (C) Annotation enrichment analysis of phosphoproteins up-regulated in either the
851 DasR or A204 parental cells compared against the human genome using the DAVID
852 application. The resultant p values of each term were $-\log_{10}$ transformed. Multiple hypothesis
853 testing was controlled using a Benjamini-Hochburg FDR threshold of 0.1.

854

855 **Figure 5. Biological function analysis of DasR versus A204 parental cells.** (A)
856 Annotation enrichment analysis of DasR and A204 parental up-regulated phosphoproteins
857 using the DAVID functional annotation tool. Network maps represent clusters of annotation
858 terms from different databases with associated function. Nodes represent each term and the
859 connecting line their association; line thickness is number of overlapping proteins. The inner
860 and outer node are DasR and A204 parental datasets respectively. Node size represents the
861 number of proteins annotated with that term. The colour intensity of the node represents the
862 significance of enrichment and grey depicts no proteins. (B) Heat map of proteins in network
863 cluster based on the $\log_2(\text{DasR}/\text{A204})$ SILAC ratio. (C) An association network of proteins
864 from the 'insulin signalling' and 'transcription' clusters were analysed through the STRING
865 application. Red or blue coloured proteins are from the cluster lists and grey are added
866 STRING interactors. Line thickness portrays the STRING calculated association confidence.

867

868 **Figure 6. Comparative assessment of PazR and DasR cells.** (A) Venn diagram to show
869 overlap of phosphosites between the PazR and DasR datasets in at least 2 out of 3
870 biological replicates. (B) A pie chart distribution using only overlapping phosphosites of both
871 PazR and DasR. Categories include: 'Up' (at least 2-times up-regulated versus parental),
872 'down' (at least 2-times down-regulated versus parental) and 'no change' (less than 2-times
873 up-regulated and more than 2-times down-regulated). A statistical significance cut-off (p -
874 value < 0.05) was then applied and the overlap between (C) up- or (D) down-regulated (at
875 least 2-times) in PazR and DasR lines compared to A204 parental cells phosphorylation
876 sites are shown.

877

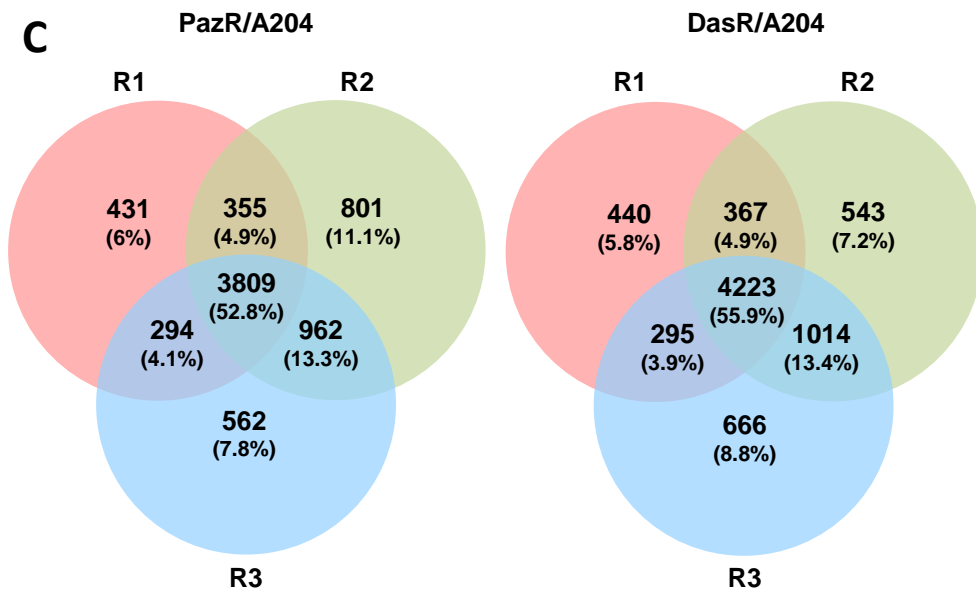
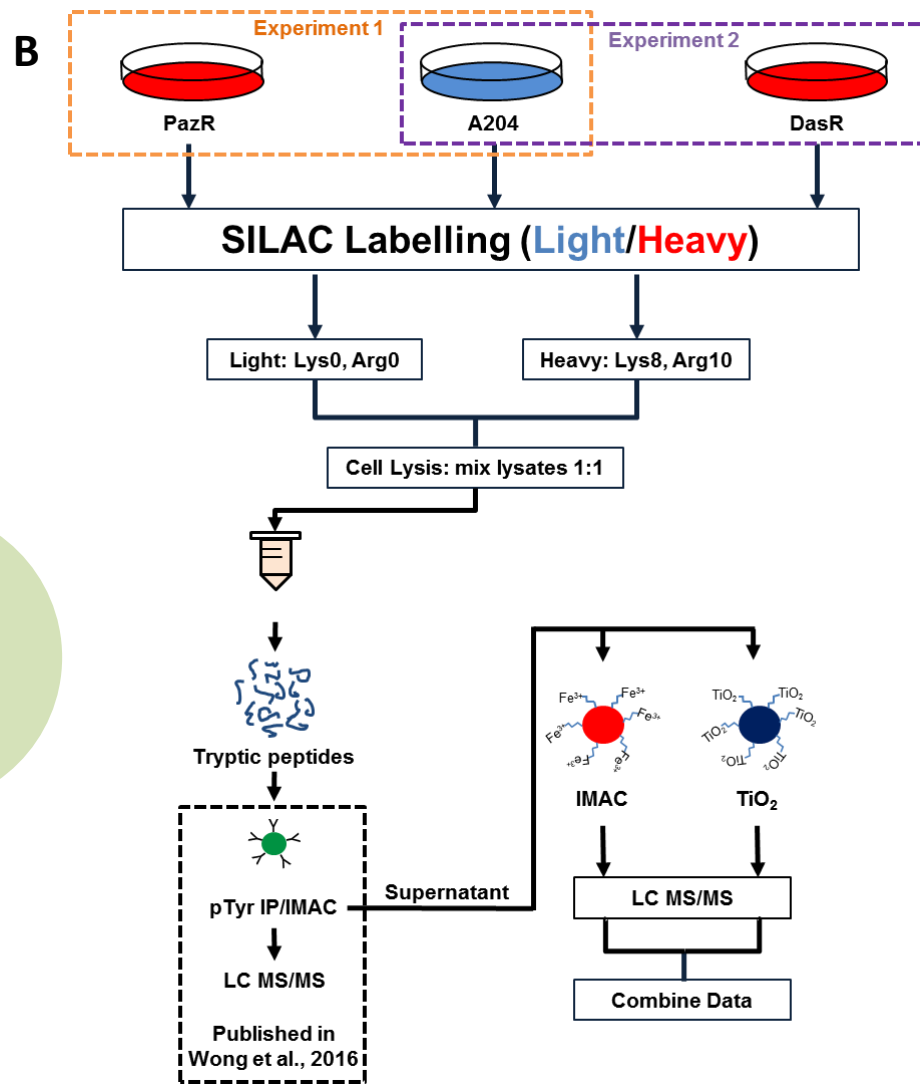
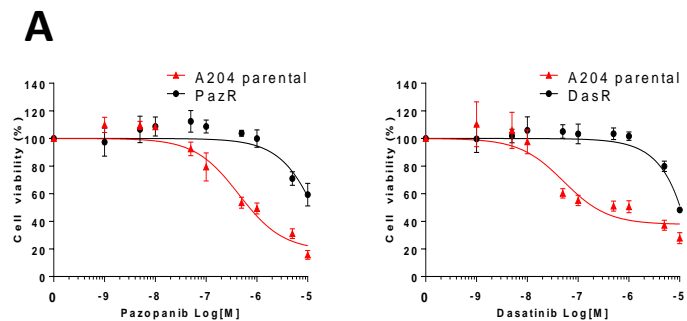
878

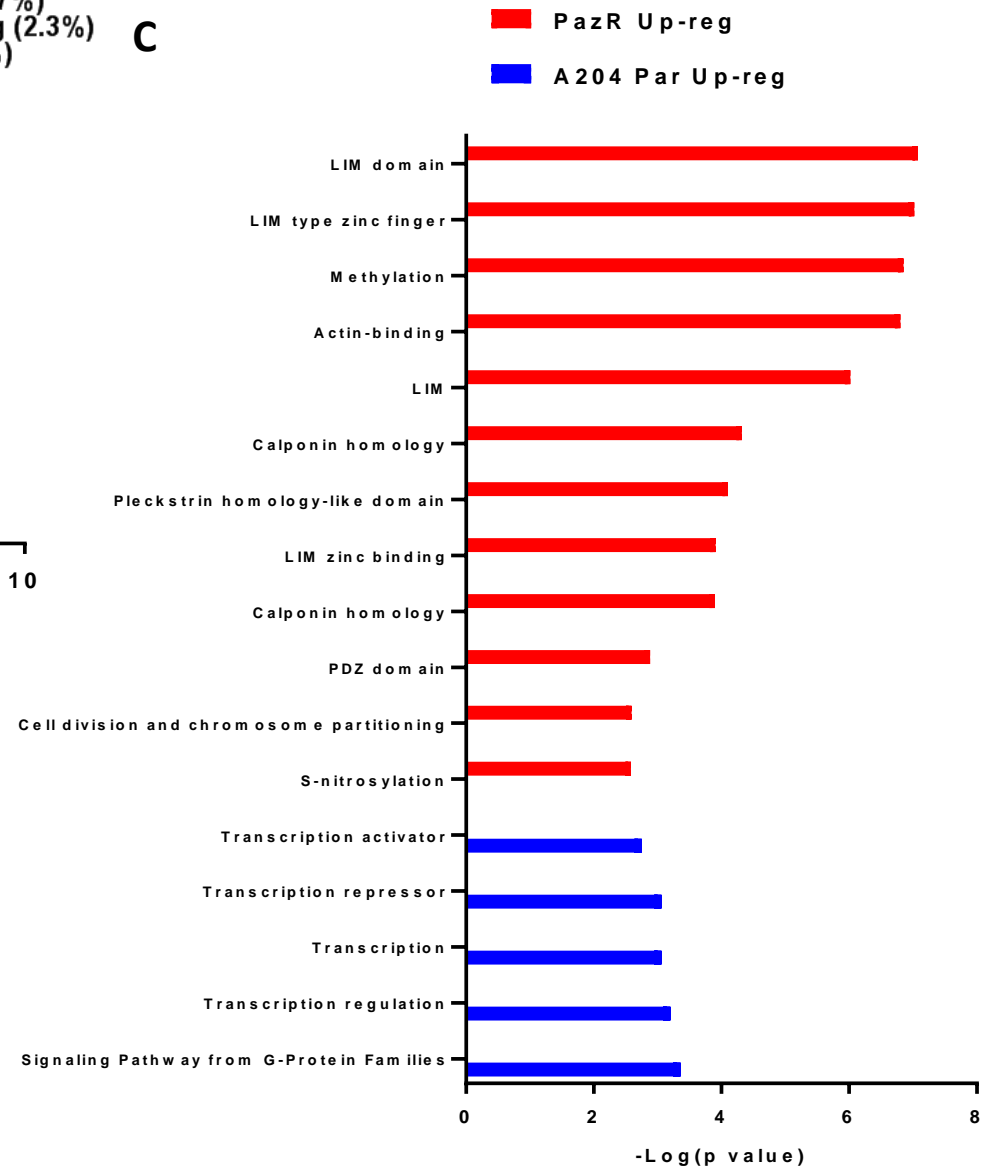
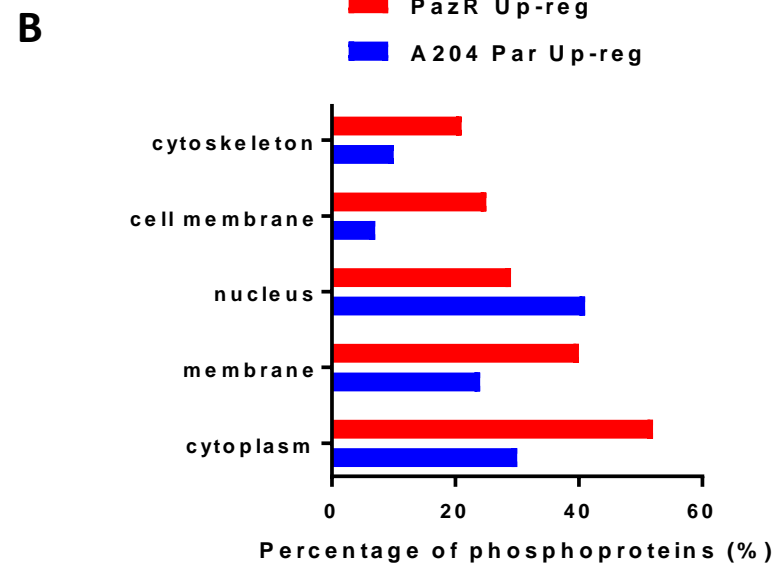
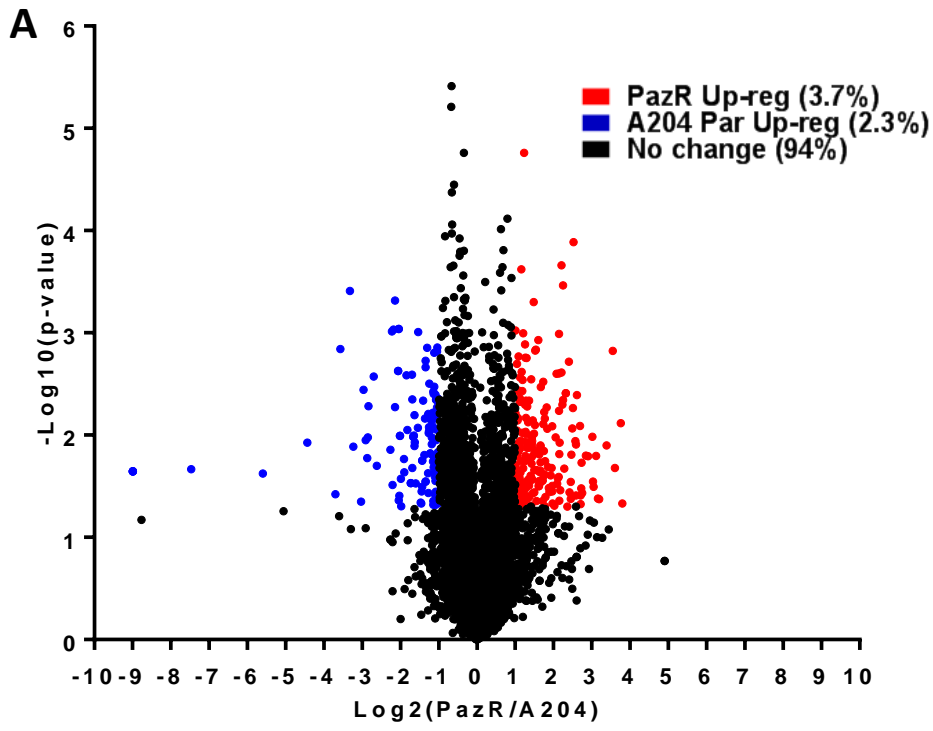
879 **Figure 7. Drug profiling analysis of in A204 parental and resistant cell lines.**

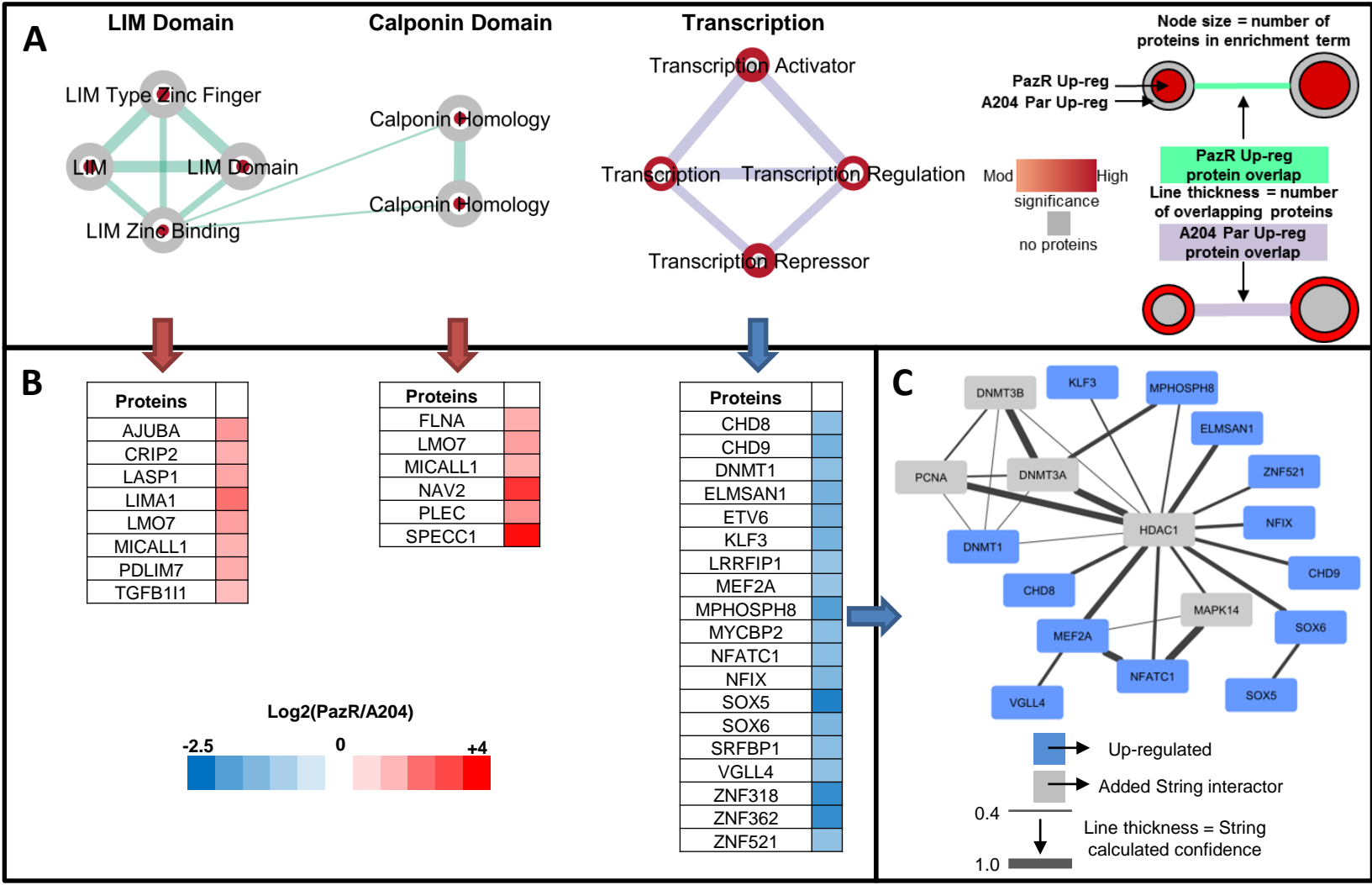
880 (A) Heatmap depicting two-way hierarchical clustering of cell viability data in drug screen.
881 A204 parental, pazopanib resistant and dasatinib cell lines were seeded in 96 well plates
882 and viability was measured using Cell Titer Glo following 72h of treatment with 28 small
883 molecule inhibitors at 100nM and 500nM (or 10nM and 50nM for NVP-AUY-922). Two-way
884 hierarchical clustering using Euclidean distance was performed. (B) Dose response curve of
885 PazR cells to pazopanib or NVP-AUY-922 treatment. (C) Dose response curve of DasR cells to
886 dasatinib or NVP-AUY-922 treatment. For (A), (B) and (C) cell viability is normalised to DMSO
887 control and values represent mean \pm SD ($n=2$ or 3). Colony formation assays comparing (A)
888 A204 parental and pazopanib resistant and (B) A204 parental and dasatinib resistant cell lines in
889 the presence of drug. Cell lines were seeded at low density (10,000 cells / well) in a 6 well plate.
890 After 2 weeks of treatment with inhibitors at the indicated doses, cells were fixed and colonies
891 were stained using crystal violet for visualisation.

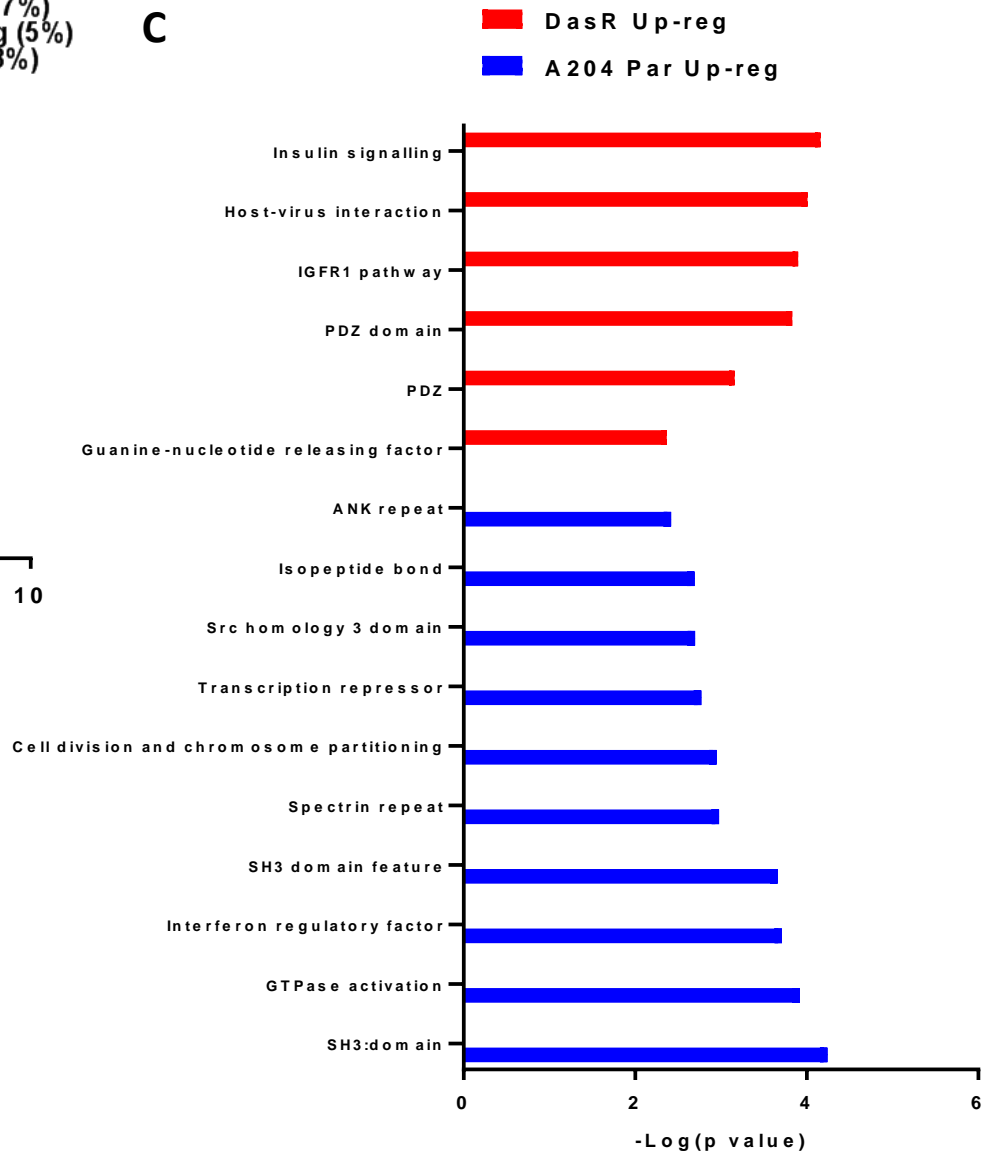
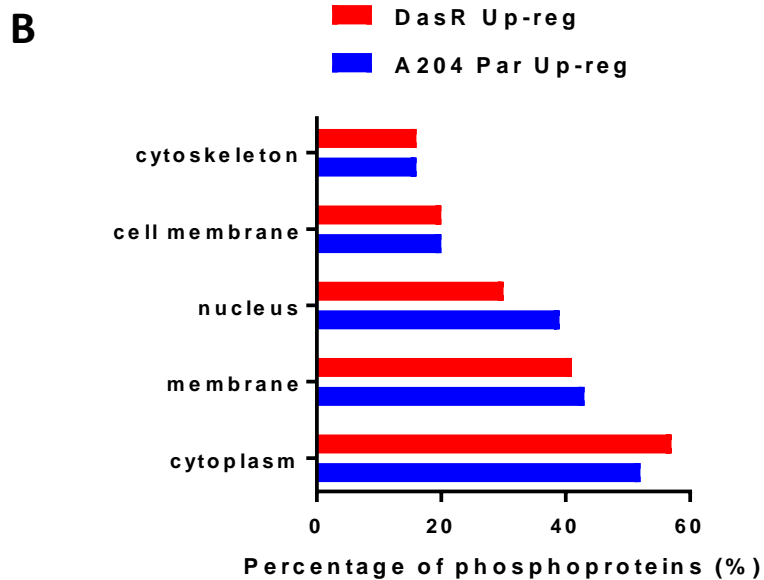
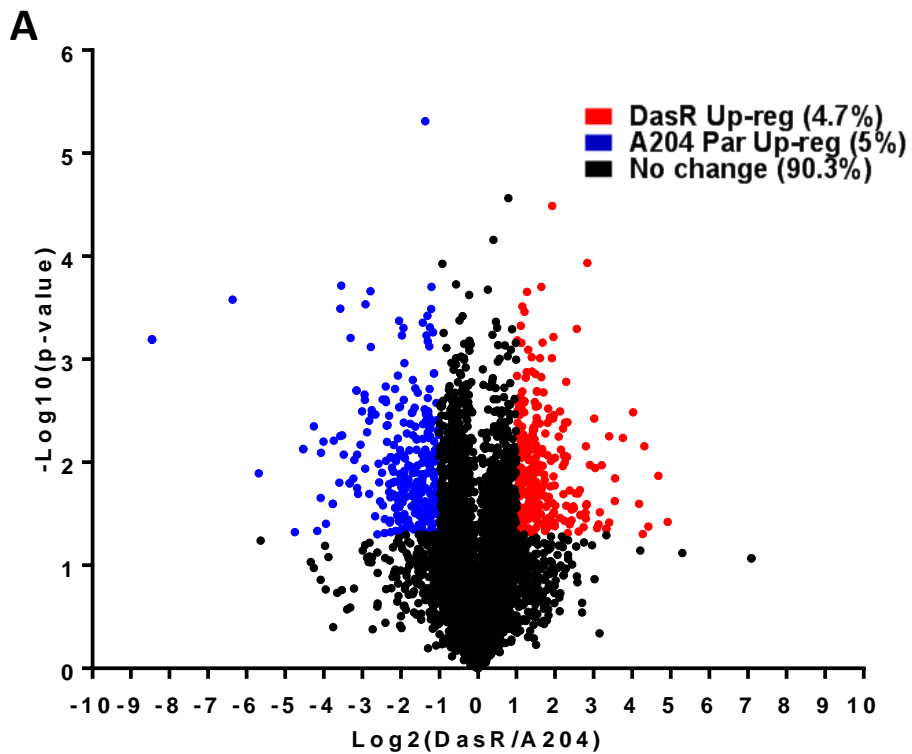
892

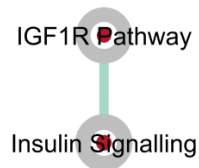
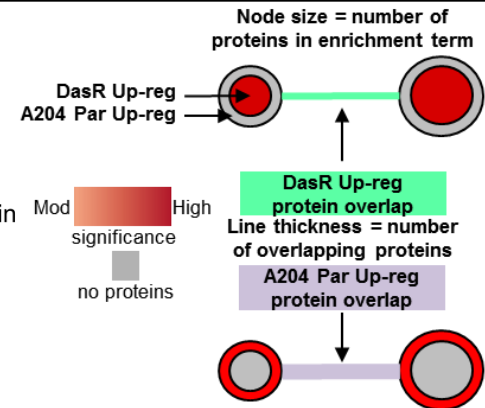
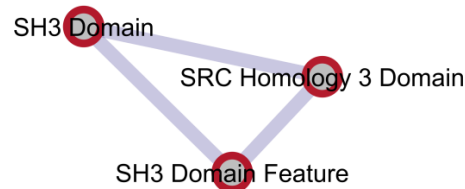
893









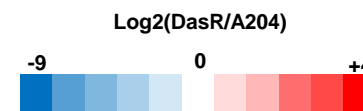
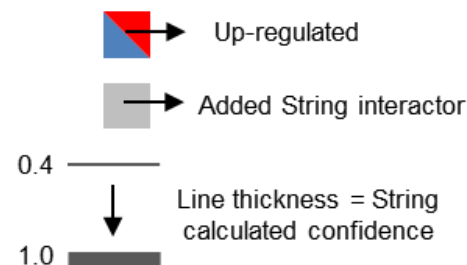
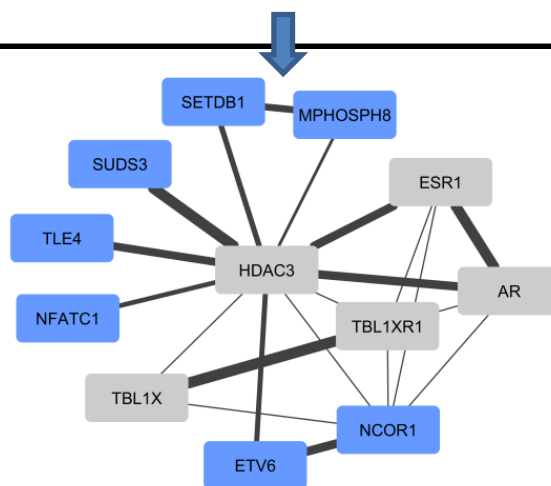
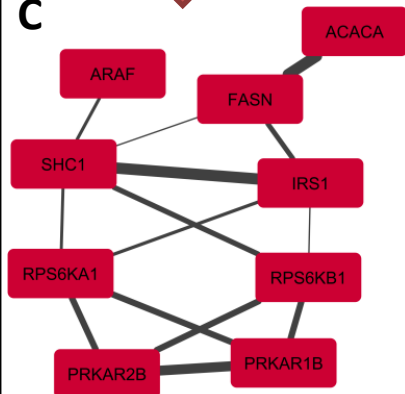
A**Insulin Signalling****PDZ Domain****Transcription****SH3 Domain****B**

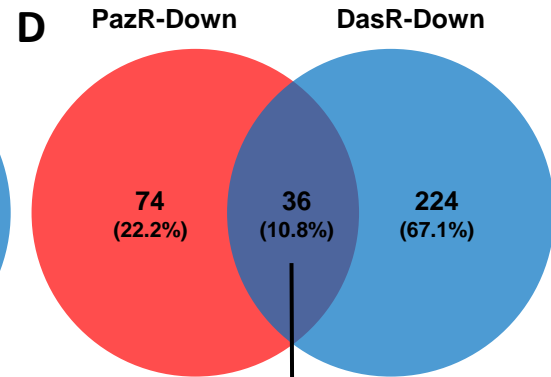
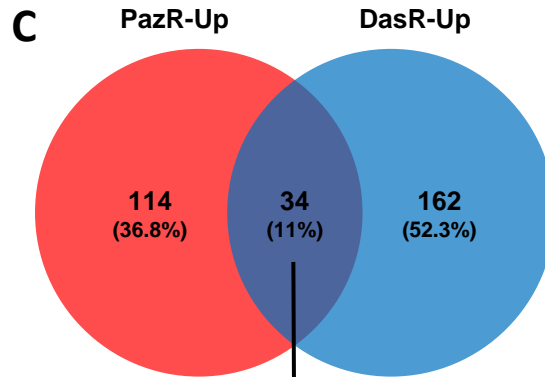
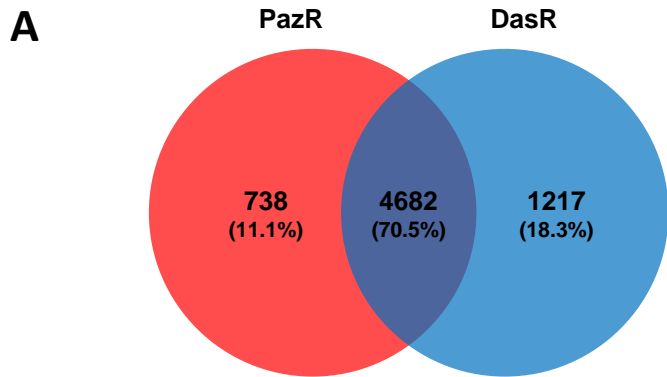
Proteins	
ACACA	
ARAF	
FASN	
IRS1	
PRKAR1B	
PRKAR2B	
RPS6KA1	
RPS6KB1	
SHC1	

Proteins	
AHNAK	
AHNAK2	
APBA1	
LMO7	
MYO18A	
SCRIB	
SLC9A3R1	
TJP2	

Proteins	
AJUBA	
ETV6	
IRF2BP1	
IRF2BP2	
IRF2BPL	
LRRFIP1	
MPHOSPH8	
NCOR1	
NFATC1	
SAMD4B	
SETDB1	
SUDS3	
TLE4	
ZNF521	

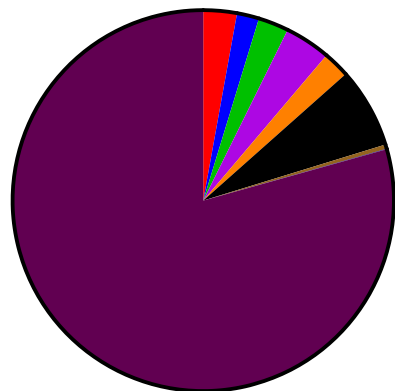
Proteins	
ARHGEF26	
ASAP1	
ASAP2	
BAIAP2L1	
DST	
FNBP1L	
NEBL	
SASH1	
SRGAP1	

**C**



B

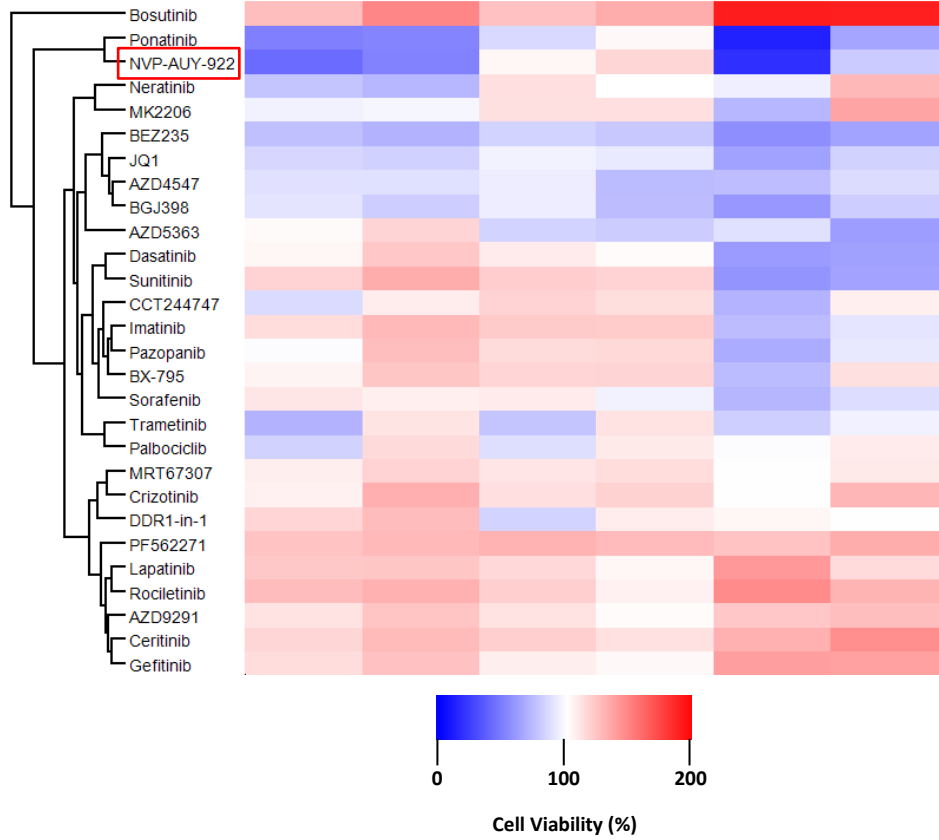
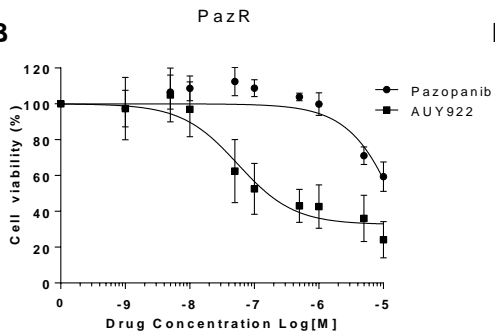
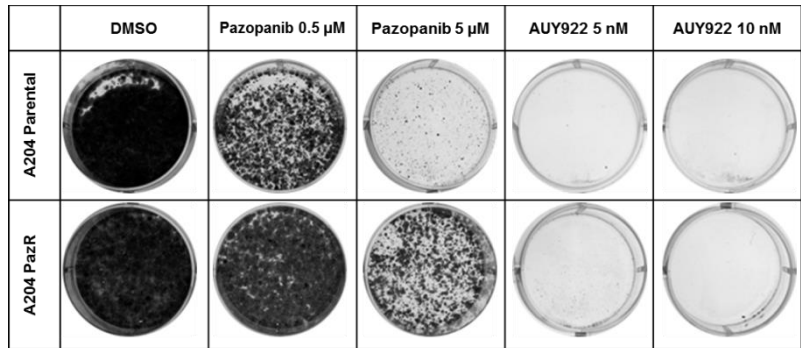
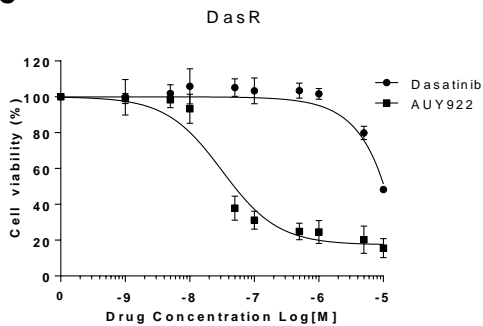
Total Dataset = 4682



- Up in PazR/Up in DasR 2.8%
- Down in PazR/Down in DasR 1.9%
- Up PazR/No change DasR 2.6%
- Up DasR/No change PazR 3.9%
- Down PazR/No change DasR 2.2%
- Down DasR/No change PazR 6.8%
- Up PazR/Down DasR 0.4%
- Up DasR/Down PazR <0.1%
- No Change 79.4%

ARID1A (S1184)
 CARHSP1 (S52)
 DBN1 (S339)
 DOS (S299)
 DSP (S2222)
 DSP (S2226)
 DTX3L (S9)
 EOMES (S107)
 HEATR9 (T328)
 IRS1 (S3)
 LIMA1 (S15)
 MAP1B (S1443)
 MAP1B (S1792)
 MAP1B (T1788)
 MPST (S17)
 MYPN (S759)
 NF2 (S13)
 PALM (S124)
 PBXIP1 (S43)
 PRKRA (S18)
 PRRT3 (S431)
 PTPN12 (S435)
 RALGPS2 (S308)
 SAMHD1 (T557)
 SCRIB (T475)
 SLC4A7 (S93)
 TNKS1BP1 (S1620)
 TNKS1BP1 (S1621)
 TNKS1BP1 (S1666)
 TNKS1BP1 (S429)
 TNKS1BP1 (S672)
 TNKS1BP1 (S836)
 TNS3 (S776)
 ZFP36L1 (S54)

AKAP6 (S1073)
 APPL1 (S401)
 ARHGEF26 (S416)
 ARHGEF26 (S419)
 ARHGEF26 (S422)
 ARHGEF26 (T417)
 BAIAP2L1 (S414)
 BICC1 (S803)
 ETV6 (S22)
 ETV6 (T18)
 FN1 (S2006)
 GNAS (S174)
 GNAS (S230)
 GNAS (S233)
 HSPH1 (S765)
 ITPKB (S174)
 ITPKB (S176)
 MAGED2 (S229)
 MEF2A (S330)
 MPHOSPH8 (S136)
 MPHOSPH8 (S138)
 NFATC1 (S220)
 PDE8A (S385)
 RCAN3;RCAN1 (S23)
 RCAN3;RCAN1 (S27)
 RIPK2 (S220)
 RPS6KA3 (S369)
 RPS6KA3 (S715)
 RTN4 (T188)
 SASH1 (S743)
 SMAP2 (S139)
 SOX6 (S358)
 SYNE1 (S8234)
 TBC1D4 (S570)
 TBC1D4 (S666)
 ZNF521 (S605)

A**B****D****C****E**